TÉCNICO LISBOA

Surface Modification Strategies for Microfluidic Devices

Patricia Alexandra Gonçalves Canané

Thesis to obtain the Master of Science Degree in

Biological Engineering

Supervisors: Drª. Vânia Cristina Henriques Silvério
Prof. Susana Isabel Pinheiro Cardoso de Freitas

Examination Committee

Chairperson: Prof. Miguel Nobre Parreira Cacho Teixeira
Supervisor: Drª. Vânia Cristina Henriques Silvério
Member of the Committee: Prof. Tiago Paulo Gonçalves Fernandes

September 2019

I declare that this document is an original work of my own authorship and that it fulfills all the requirements of the Code of Conduct and Good Practices of the Universidade de Lisboa.

Acknowledgments

I would like to thank my mother for all her support, encouragement and caring over all these years, for always being there for me through thick and thin and without whom the conclusion of my academic endeavor would not be possible. I would also like to thank my boyfriend for all his patience, motivation and for always believing in me, even in the hardest of times.

I would also like to acknowledge my dissertation supervisor Drª Vânia Silvério for going above and beyond for me throughout this project. Her dedication and hard-work were (and are) a great inspiration.

I would also like to thank my friends Sara, Sofia and Marta that helped me grow as a person and were always there for me, even in my worst days.

Last but not least, to the great team of INESC-MN, where patience, will to help and availability greatly contributed to the development of this project.

To each and every one of you – Thank you.

Abstract

Microfluidics provides a portable, cost-effective, rapid and low consumption alternative to the typical laboratory instruments for biological detection. Microfluidic devices benefit from microfabrication techniques, which allow the design of complex nano/micro-scale structures. However, high surface to volume ratio generates problems of biofouling, unwanted cell behaviour and surface-surface adhesion, jeopardizing the efficiency of microfluidic and microfabrication techniques. Chemical or physical surface wettability modification (SWM) is an expedite method to tailor adhesion forces. In this work, silanization with HMDS, FDTS and APTES by Room Temperature Chemical Vapor Deposition (RT-CVD) was applied in samples of silicon, glass, PDMS, SU-8 photoresist, thermoplastics (PET, PS and PMMA) and thin films (gold, silicon dioxide and alumina). Deterministic Roughness was implemented in silicon dioxide thin films ($CA_{t0} \simeq 80°$), by crafting square structures on the substrate. SWM was assessed by measurements of liquid-solid Contact Angle (CA). Hydroxyl (-OH) containing surfaces ($CA_{t0} < 20°$), subjected to RT-CVD exhibited an increase in CA ($70° < CA < 100°$) due to establishment of silane-surface covalent bonds and exposure of non-polar groups. Functionalization of gold films ($CA_{t0} \simeq 80°$) with FDTS ($CA \simeq 100°$) and APTES ($CA \simeq 40°$) was also observed. Functionalization of PDMS substrates and SU-8 was achieved, but the hydrophobic behaviour persisted. Thermoplastics ($CA_{t0} \ll 80°$) showed a decrease in wettability ($80° < CA < 100°$) after exposure to FDTS and APTES, without establishment of silane-substrate covalent bonds. XPS analysis of alumina thin films indicated the presence of hydrogen-bonded APTES molecules. Implementation of square structures of varied size (1-5 μm) and spacing (2-5 μm) lead to an increase in CA up to 35$\%$.

Keywords

Surface tailoring, Room Temperature Chemical Vapor Deposition, Surface Roughness, Contact angle.

Resumo

A Microfluídica fornece alternativas portáteis, de baixo consumo, custo e tempo de análise, às técnicas usadas em laboratório para biodetecção. A produção de dispositivos microfluídicos requer técnicas de microfabricação, que permitem o desenho de estruturas à nano/micro-escala. Contudo, o alto rácio superfície/volume gera problemas de adesão indesejada entre analitos-substrato e substrato-substrato, comprometendo a eficiência de análise e fabricação. A modificação da molhabilidade de superfície (MMS), química ou física, é uma forma expedita de customizar forças de adesão. Neste trabalho, amostras de silício, vidro, PDMS, SU-8, termoplásticos (PET, PS e PMMA) e filmes finos (de ouro, dióxido de silício e alumina) foram expostas a HMDS, FDTS e APTES por Deposição de Vapor Químico à Temperatura Ambiente. Rugosidade determinística foi implementada em amostras de SiO_2, por microfabricação de quadrados de diversos tamanhos (1-5μm) e espaçamento (2-5μm). A MMS foi avaliada por medidas de ângulos de contacto (AC). Superfícies com grupos hidroxila ($AC_{t0}<20°$) sofreram uma diminuição da molhabilidade ($70°<AC<100°$) devido a exposição de grupos apolares. Functionalização de filmes de ouro ($AC_{t0}\simeq80°$) com FDTS ($AC\simeq100°$) e APTES ($AC\simeq40°$) foi observada. A silanização de amostras de PDMS e SU-8 foi obtida, apesar do comportamento hidrofóbico perdurar. Uma diminuição da molhabilidade foi observada nos termoplásticos ($AC_{t0}\ll80°$) após deposição de FDTS e APTES ($80°<AC<100°$). Análise por XPS indicou a presença de moléculas de APTES nos filmes de alumina, ligadas por pontes de hidrogénio. Implementação de rugosidade determinística gerou uma diminuição da molhabilidade em 35$\%$.

Palavras Chave

Mdificação de Superfícies, Deposição de Vapor Químico à Temperatura Ambiente, Rugosidade de Superfície, Ângulo de Contacto

Contents

List of Figures

List of Tables

Nomenclature

Greek Symbols

ΔP	Laplace pressure
γ_{lv}	Liquid-vapor interface energy
γ_{sl}	Solid-liquid interfacial energy
γ_{sv}	Solid-vapor interfacial energy
γ	Surface tension
θ_C	Cassie-Baxter's contact angle
θ_W	Wenzel's contact angle
θ_Y	Young's contact angle

Latin Symbols

A_{aw}	Horizontal projected area
c	Capillary constant
d	Spacing between the squared structures
F	Vertical force felt on a droplet on top of a crevice
f	Fraction of the projected area that is wet
L	Lateral size of the squared structures
P_{liquid}	Liquid Pressure
P_{air}	Air pressure
r	Roughness value of the solid

r_r	Roughness value of the wet area
R_1, R_2	Principal radii of curvature at any point of the droplet

Acronyms

APTES	(3-aminopropyl) triethoxysilane
BE	binding energy
CB	Cassie-Baxter
CVD	Chemical Vapor Deposition
CA	Contact Angle
DI	Deionised
ELISA	Enzyme-Linked Immusorbent Assays
ESCA	Electron Spectroscopy for Chemical Analysis
FDTS	Perfluorodecyltrichlorosilane
GAPDH	Glutaraldehyde-3-Phosphate-Dehydrogenase
HMDS	Hexamethyldisilazane
LOC	Lab-on-chip
LBADSA	Low-Bond Axisymmetric Drop Shape Analysis
MEMS	Micro-electro-mechanical systems
NP	Nanoparticles
PBS	Phosphate-Buffered Saline
PCR	Polymerase Chain Reaction
PDMS	Polydimethylsiloxane
PET	Polyethylene Terephthalate

PMMA	Poly(methyl methacrylate)
PR	Photoresist
PS	Polystyrene
RFGD	Radio-Frequency Glow Discharge
ROS	Reactive Oxygen Species
RT-CVD	Room Temperature Chemical Vapor Deposition
SAM	Self-Assembled Monolayer
SF	sensivity factors
Si	Silicon
SWM	Surface Wettability Modification
TOA	take-off angle
XPS	X-ray Photoelectron Spectroscopy

1

Introduction

Contents

1.1 Brief Introduction to Surface Wettability Modification

Microfluidic devices have attracted great attention in diverse fields of industry and research, such as biology, biomedical and chemistry [1–3], due to their portability, low detection time and reagent consumption, control of heat and mass transfers and possibility of multi-step processes. These devices offer a precise and controlled environment for studies of cell-growth and proliferation, being a cost-effective and compact alternative to the conventional biological laboratory methods [4]. The construction of these nano/micro-scale devices relies on microfabrication techniques (such as photolithography).

Microfabrication offers the possibility for highly reproducible mass-fabrication of devices with complex geometries and functionalities for biological detection and drug delivery systems, sensor and electronics integration, such as Lab-on-chip (LOC), Micro-electro-mechanical systems (MEMS) and BioMEMS devices. However, available microfabrication procedures, production time and cost must be considered, making the choice of substrates a major step in microfabrication and microfluidic design. Plus, due to the characteristic high surface to volume ratio of microfluidic devices, forces such as adhesion, cohesion and surface tension greatly impact the efficiency of the system, where the flow and interaction of bioanalytes is of extreme importance. If the microfluidic channels are hydrophobic (or repel water as, for example, Polydimethylsiloxane (PDMS) elastomer), surface wettability will be low, which will hinder the flow of the liquid. This will make the process more expensive, as a more powerful pump will be required to reach the desired flow rate. Furthermore, it is well established that surface properties such as roughness and chemical composition (which impact surface wettability) have a profound influence on cell behavior and adhesion [5].

Silicon (Si), glass (both hydrophilic surfaces), PDMS elastomer and SU-8 Photoresist (PR) (both hydrophobic surfaces) are the most commonly used substrates in fabrication of microfluidic devices for biological application [6–9] due to their good surface stability, chemical compatibility, low cost (except for Si) and biocompatibility. Thermoplastics (such as Polyethylene Terephthalate (PET), Polystyrene (PS) and Poly(methyl methacrylate) (PMMA)) are an interesting choice of material for fabrication of microfluidic devices and medical implants due to their low electrical conductivity, high chemical stability and infinite possibilities of design [10, 11]. Another type of substrate used in microfluidics and other microfabricated devices are thin films (e.g. gold, silicon dioxide and alumina), due to their biocompatibility, conductivity and chemical resistance, being commonly used in the form of Nanoparticles (NP) for biosensing, drug delivery and immunotherapy [12–14]. However, the wettable character of the materials mentioned is not always adequate for biological application, impacting cell behavior and morphology. As an example, biofouling (or non-specific adhesion of proteins and cells), consequent of surface hydrophobicity, is a great concern needing solution in biological assays and biomedical implants, impacting the success of detection and implant acceptance. Furthermore, adhesion forces between materials used in microfluidics may compromise the microfabrication techniques necessary to achieve the wanted design. For

example, SU-8 photoresist masters are used for fabrication of PDMS structures, where a peeling step of the two materials is required. However, the surface chemistry of PDMS and SU-8 increases the difficulty of peeling, due to hydrogen bonds and van der Waals forces that lead to a high adhesion and, sometimes, damage to the microfluidic structure [15]. Therefore, surface wettability of the chosen substrates for fabrication of biodetection devices must be accounted for and if needed, modified, to guarantee a successful application.

Surface Wettability Modification (SWM) is a very useful tool to suit the wettable behavior of materials, solving problems of unwanted stiction between materials, adhesion between biomolecules and surfaces and even facilitating the flow in microfluidic devices. This approach is gaining great interest, as it enables the use of several promising materials in need on diverse fields, such as biology and biomedical [16–19], microfabrication [20, 21] or microfluidics [22, 23] which would otherwise not be addressed.

Wettability is understood as the ability of a liquid to maintain contact with a solid surface, which is a consequence of the balance between intermolecular interactions of adhesive type (liquid to surface) and cohesive type (liquid to liquid) [24]. The influence of these forces for a certain liquid-solid pair can be perceived by the resultant Contact Angle (CA) (fig. 1.1), often symbolized by θ.

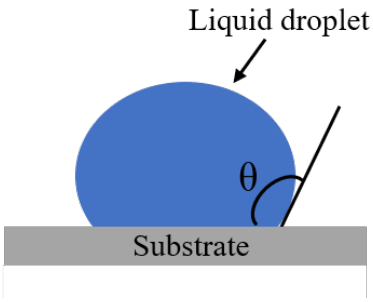

Figure 1.1: Contact angle (θ) is defined as the interior angle of a liquid droplet in contact with a solid substrate.

SWM can be achieved by altering the chemical exposed groups of a surface or its roughness, which can be stochastic or deterministic. By considering only the exposed groups and their polarity, the contact angle can be evaluated by the Young model of wettability, where only interfacial forces are considered. By modifying the roughness of the surface, other factors must be considered, taken into account in the Cassie-Baxter and Wenzel models, explained in detail in chapter 2.

A practical, efficient and cost-effective method to chemically alter surface wettability is Room Temperature Chemical Vapor Deposition (RT-CVD), which consists in the deposition of a vapor-phase of a chemical agent, under specific pressure and room temperature conditions. If the chemical agent is adequate, a chemical reaction occurs between the molecules of the agent and the chemical exposed groups on the surface of the material, leading to a certain molecular conformation that impacts surface wettability. On the other end, surface roughness can be altered by several chemical and physical metho-

ds resulting in stochastic or deterministic roughness. Tailoring the deterministic roughness can be obtained through microfabrication techniques, such as a photolitographic process, as described in chapter 3. Deterministic roughness brings the advantage of control of the structure's dimensions, and thus, reproducibility, in contrast to the usage of stochastic roughness obtained, for example, with femtosecond laser irradiation [25].

1.2 Proposed Work

In this work, a chemical and physical method for SWM were studied. Chemical SWM consisted on the silanization of surfaces commonly used in microfluidics (silicon, glass, PDMS elastomer and SU-8 photoresist), thermoplastics (PET, PS and PMMA) and thin films (of gold, alumina and silicon dioxide) with exposure to HMDS, FDTS and APTES vapor by RT-CVD.

Physical SWM consisted on the design of square patterns (deterministic roughness) on silicon dioxide thin films, using a photolithographic process.

The assessment of chemical and physical SWM was performed by measurements of contact angle of deionised water droplets and Phosphate-Buffered Saline (PBS) droplets in contact with the (chemically or physically) modified substrates. Contact angles were measured with Image J software with Low-Bond Axisymmetric Drop Shape Analysis (LBADSA) plugin.

PET substrates and alumina thin films exposed to APTES by RT-CVD for 30 min were submitted to X-ray Photoelectron Spectroscopy (XPS) analysis, to confirm the presence of silane molecules on the surface and possible molecular orientation adopted following interaction with the exposed groups at the PET and alumina substrates.

1.3 Organization of the Document

This work is composed by five chapters. Chapter 2 consists on an introduction to surface wettability, where the phenomena of wettability, surface tension and contact angle are described. The theoretical models of surface wettability (Young, Cassie-Baxter and Wenzel models), chemical and physical methods for SWM are also presented in this chapter. The experimental techniques used in this work, including the microfabrication of thin films, rough surfaces, system used for silanization by RT-CVD, CA measurement and XPS analysis are described in chapter 3. In chapter 4, contact angle and XPS data evaluation consequent of chemical and physical SWM is performed. A final remark considering the techniques used for SWM and future scientific work are presented in chapter 5.

2

Wetting, Roughness and Chemical Functionalization

Contents

2.1 Wetting behavior and contact angle

Wetting is understood as the ability of a liquid to maintain contact with a solid surface, resulting from intermolecular forces such as adhesion and cohesion, established upon liquid-solid interaction. Adhesion forces are responsible for the spreading of a liquid in a solid surface, reflecting the attractive liquid-solid forces. Cohesion forces, such as hydrogen bonds, dipole interactions, proton exchange and van der Waals, represent the attraction between the molecules within the liquid. If adhesion forces surpass cohesive forces, the liquid will spread over the surface (fluidophilic surface). If the cohesive forces surpass the adhesion forces, the liquid is repelled by the surface (fluidophobic surface) [26]. In a ideal liquid, each molecule of the liquid is pulled equally in every direction by nearby liquid molecules, resulting in a null net force. However, liquid molecules at the top of the bulk are not evenly surrounded by other liquid molecules to provide a balanced net force. Thus, these molecules are pulled inward, creating an internal pressure (fig. 2.1).

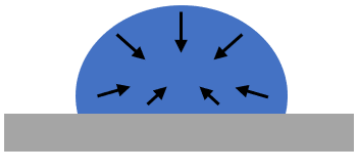

Figure 2.1: Unbalanced forces of liquid molecules at the liquid-air interface generate the surface tension, giving shape to the droplet (adapted from Yuan, Y. *et al*, 2013).

As consequence, contraction of the surface area of the liquid occurs to maintain the lowest surface free energy. This intermolecular force to contract the surface of the liquid is known as surface tension and it's the major phenomena responsible for the shape of drops. Surface tension and surface free energy or interfacial energy are two interconnected concepts. Surface energy can be defined as the energy difference between the bulk and the surface of the material and is the energy required to create one unit of new surface area. The combination of surface tension, interfacial energies (liquid-solid-vapor) and external forces, the latter of lower impact, define the contact angle, which is specific for the pair liquid-surface. The contact angle is defined as the internal angle formed between the liquid-solid and vapor-solid interfaces and the interface were liquid-vapor-solid co-exist is referred as the "three-phase contact line" [27]. A high wettability or high surface energy is characterized by a contact angle $\theta < 90\ ^\circ$ (in this case the sample is called hydrophilic, fluidophilic or lyophilic surface). A low wettability or low surface energy leads to a contact angle $\theta > 90\ ^\circ$ (hydrophobic, fluidophobic or lyophobic surfaces). Surfaces with contact angles $\theta < 5\ ^\circ$ are designated as superhydrophilic, while values of CA $\theta > 150\ ^\circ$ are called superhydrophobic surfaces (fig. 2.2).

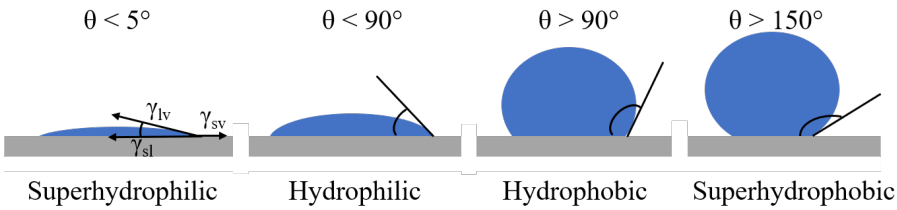

Figure 2.2: Illustrations of contact angles formed by sessile liquid drops on a flat, rigid surface (adapted from Yuan, Y. *et al*, 2013).

The Young equation expresses this as:

$$cos(\theta_Y) = \frac{\gamma_{sv} - \gamma_{sl}}{\gamma_{lv}} \tag{2.1}$$

where θ_Y is the Young's contact angle, γ_{lv} is the liquid-vapor interface energy,γ_{sv} is the interfacial energy between solid surface and vapor and γ_{sl} is the solid-liquid interfacial energy. The Young equation was established for rigid, smooth surfaces, considering that the effect of surface roughness on adhesion forces cannot surpass the effect of chemical groups present on the surface. If the degree of roughness is high enough to surpass the chemical effect of the surface wettability, then surface roughness needs to be accounted for.

The Wenzel model (eq. 2.4) includes the roughness value of the solid, $r > 1$ (eq. 2.2), defined as the ratio between the rough area of the surface (A_r) and the projection (or apparent) area (A_a) [28, 29]. The Cassie-Baxter model (eq. 2.5) includes the fraction f (< 1), of solid surface that is wet (eq. 2.3), the fraction of air gaps (1 - f) and the contact angle on the gas in the gaps (θ_X) which is considered to be 180°. These parameters are illustrated in fig. 2.3.

$$r = \frac{A_r}{A_a} > 1 \tag{2.2}$$

$$f = \frac{A_{structuredtop}}{A_{repeatinglattice}} < 1 \tag{2.3}$$

The contact angle θ is then obtained from the Young contact angle θ_Y as follows:

$$cos(\theta_W) = rcos(\theta_Y) \tag{2.4}$$

$$cos(\theta_C) = fcos(\theta_Y) + (1 - f)cos(\theta_X) \tag{2.5}$$

The two equations can be combined to produce a more general equation (eq. 2.6) to cover the case when the contacting areas are not smooth, thus considering the roughness value of the wetted area

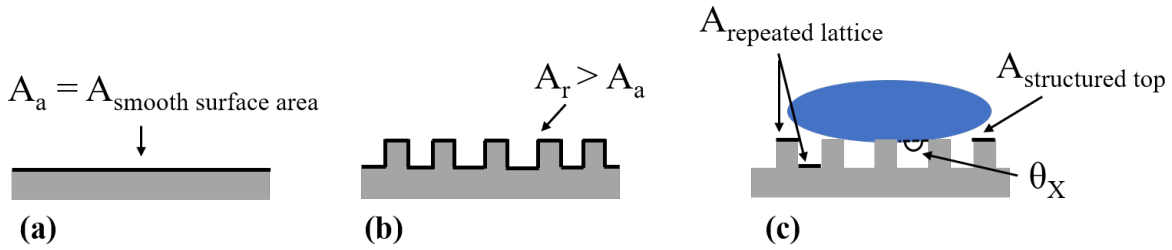

Figure 2.3: Illustration of the **(a)** apparent area A_a or smooth surface area, **(b)** rough area A_r, **(c)** area of repeated lattice $A_{repeatedlattice}$ and superficial area of the structured pattern $A_{structuredtop}$.

(r_r) :

$$cos(\theta_C) = r_r f cos(\theta_Y) + f - 1 \tag{2.6}$$

The Wenzel contact angle, θ_W, corresponds to the wetting mode where all the rough solid surface is wet. This model suggests that a hydrophilic surface becomes more hydrophilic with the increase of the roughness of the solid, while a hydrophobic surface becomes more hydrophobic. As for the Cassie-Baxter contact angle, θ_C, it is assumed that only a partial area of the microstructure gets wet, whereas air is trapped beneath the liquid. (fig 2.4). Thus, a decrease in surface wettability is observed.

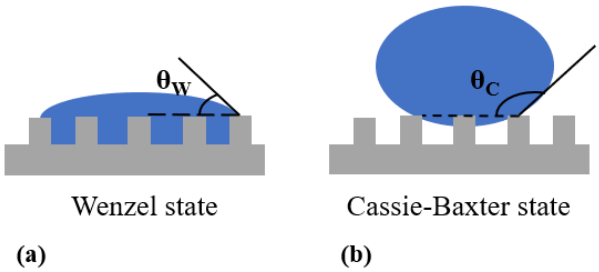

Figure 2.4: Illustrations of **(a)** the Wenzel and **(b)** Cassie-Baxter state for a liquid droplet onto a rough surface (adapted from Gert H. *et al*, 2015).

The influence of surface roughness in cell behavior is an growing field of study, as biofouling is one of the major problems in biomedical implants and biological assays. As an example, Mussano F. and co-workers [30] studied the effects of different roughness of alumina surfaces on osteoblast response. For that, the authors used oxidative anodization to generate two alumina surfaces with different pore diameters (the range varied from 16 to 30 nm and 65 to 89 nm). In *vitro*, cell response was studied in terms of cell adhesion, viability and morphology. Both alumina surfaces promoted higher cell adhesion and viability than the control condition represented by the standard polystyrene culture dish. These results enhance the importance of surface roughness as a method to control cell behavior.

2.2 Chemical Functionalization

2.2.1 Polar vs Non-polar Surface Groups

SWM can be achieved, for example, by chemically altering the exposed groups of a given surface. Chemical functionalization requires the usage of an adequate agent with specific functional groups that effectively impact surface wettability. This impact relies on the polarity of functional groups. When using water or a water-based solutions, exposed polar groups on the surface such as hydroxyl (-OH) groups are responsible for high surface energy or high wettability ($\theta < 90°$), while apolar groups, such as hydrocarbons (C_nH_{2n+1}) generate low surface energy or low wettability ($\theta > 90°$) [31]. Therefore, if a change in wettability is required, one must evaluate the type of exposed groups on the surface and decide which functional groups are most suited for the final application. Silanes are the most commonly used chemical agents for SWM and the process of chemically altering surfaces with these agents is designated as silanization. A successful silanization usually requires the presence of hydroxyl groups at the surface due to the high affinity of silane head groups to polar groups. In this scenario, the exposure of a high number of functional groups present in silane molecules is assured.

2.2.2 Silanes

Silanes are amphiphilic functional molecules with the general formula X-$(CH_2)_n$-Si$(R)_m$ where X represents the functional group, $(CH_2)_n$ is a flexible spacer and Si$(R)_m$ are the anchor groups that can react with the exposed groups of the substrate (fig. 2.5a). Choosing a silane depends on the type of surface chemistry and the aim of surface modification. For example, APTES (3- aminopropyl)triethoxysilane) is the most commonly used silane for biological applications, due to its biocompatibility, as it enables the attachment of organic components to inorganic surfaces.

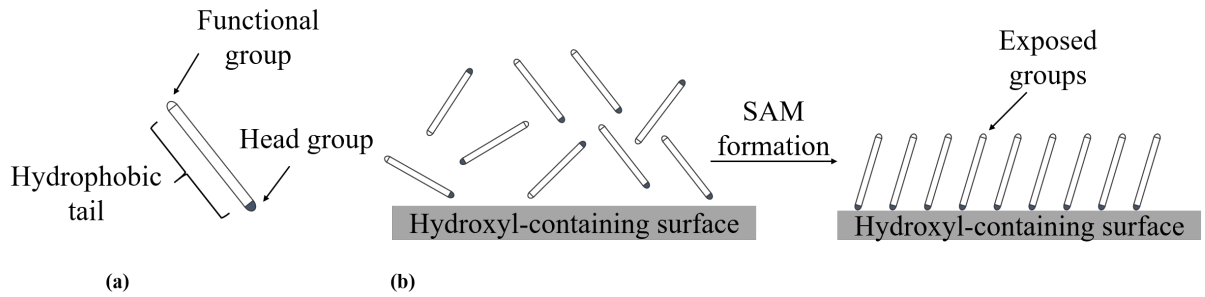

Figure 2.5: Scheme of **(a)** a silane molecule with a reactive head group, hydrophobic tail and functional group. The exposure of a hydroxyl-containing surface to reactive silane molecules **(b)** results in the formation of a self-assembled monolayer consequent of a covalent reaction (adapted from Colorado Jr., R., Lee, T. R., 2001).

If the reaction occurs between the silane molecules and the exposed groups at the surface, a Self-

Assembled Monolayer (SAM) is formed (fig. 2.5b). SAM is a structure composed of organic molecules, in liquid or gas phase, that are spontaneously bound to a surface normally due to covalent bonds formed between the head group of the amphiphilic molecule (fig.2.5) and the exposed groups of the substrate [32]. The quality of SAM layer relies on the stability of the covalent bonds established between the silane and the surface and the orientation adapted by the silane molecules after reaction. If a vertical orientation of the silane molecules is achieved, a close-packed monolayer is formed, which leads to a more uniform SWM across the surface.

There is a large variety of silanes available, with distinct tail lengths, functional and head groups. This variety enables the selection of an adequate functional group to fulfil a specific goal, such as binding a specific bioanalyte to a surface which wouldn't otherwise happen. In this work, three silanes were employed as chemical functionalization agents: hexamethyldisilazane (HMDS), perfluorodecyltrichlorosilane (FDTS) and (3-aminopropyl)triethoxysilane (APTES).

2.2.2.A HMDS

Hexamethyldisilazane (HMDS) silane, with the chemical formula $HN[Si(CH_3)_3]_2$, has trimethylsilanol (-$Si[CH_3]_3$) groups as functional groups and an amino group as the reactive group (fig.2.6a). This chemical agent reacts with hydroxyl (-OH) groups present in the surface, leaving non-polar methyl (-CH_3) groups attached to it by covalent bonds, with release of ammonia (NH_3) (fig. 2.6b). This reaction decreases surface hydrophilic behaviour, which is observed by the increase of contact angle.

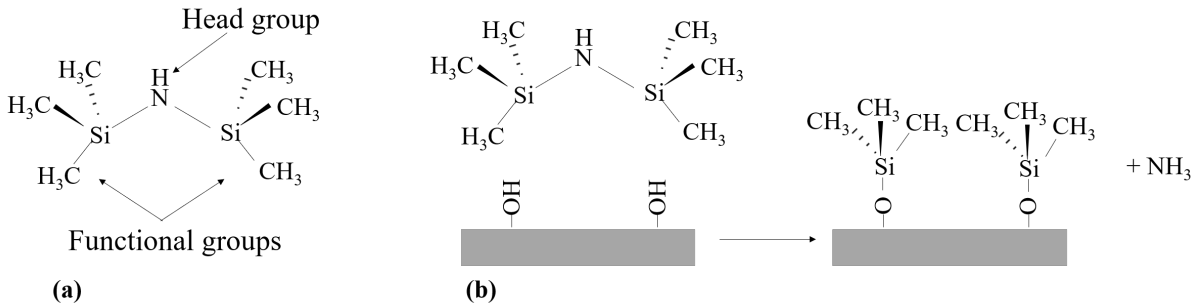

Figure 2.6: Scheme of **(a)** HMDS molecule with -NH as the head group and $Si(CH_3)_3$ as the functional groups and **(b)** a covalent reaction between HMDS silane and a hydroxyl-containing surface (adapted from Silverio, V. *et al*, 2019).

Typically HMDS is used in photolithographic processes, to promote the adherence of both negative or positive PR added by a spin-coating process to Silicon (Si) wafers. Since Si is a hydrophilic material, the adhesion forces of photoresists (usually hydrophobic materials) to it are very low. If a primer is not applied before the PR spin-coating process, the cohesion forces of the PR surpass those of adhesion to the Si surface and the PR contracts following the spreading on the surface. Therefore, a priming step of the silicon wafer with HMDS is employed, allowing the PR to wet the Si wafer and to efficiently

adhere [33]. HMDS silane may also be employed in biological applications. Felbel, J. *et al* [34] evaluated the effect of silanization of silicon surfaces to facilitate micro Polymerase Chain Reaction (PCR). PCR is a technique widely used in molecular biology, which relies in thermal cycles to amplify specific DNA sequences. Due to the high surface to volume ratio, typical biological procedures flows at the micro and nanoscale, such as PCR in flow-through chip devices, are negatively impacted by unwanted adhesion of biomolecules. As such, the authors studied the ability of several silanes (including HMDS) to prevent the inhibition of PCR reaction of the Glutaraldehyde-3-Phosphate-Dehydrogenase (GAPDH) gene for 25 thermocycles (cycles with a denaturation step of 20 s at 94℃, annealing step of 20 s at 50℃ and primer extension for 40 s at 68℃). The first cycle started with a denaturation step of 40 s and last cycle ended with a elongation step of 100 s. The authors concluded that inhibition of PCR reaction was related to the density of hydroxyl (-OH) groups exposed at the silicon and glass chip surfaces. By pretreating the surface with HMDS, an improvement in biocompatibility was observed, effect that lasted for 25 thermocycles ($\simeq$ 34,7 min).

Other materials commonly used in microfabrication of microfluidic devices such as PDMS may also benefit from chemical exposure to HMDS silane for SWM. As example, Jankauskaite, V and co-workers [35] studied the effects of plasma polymerized hexamethyldisilazane (pp-HMDS) in wettability of PDMS, by Arc Discharge. Using this one-step film deposition method, methyl groups were added to the PDMS surface, attributing a superhydrophobic behaviour to the material as the CA increased from 122° to 170°.

2.2.2.B FDTS

Perfluorodecyltrichlorosilane (FDTS) is a silane with the chemical formula $CF_3(CF_2)_7(CH_2)_2(SiCl_3)$ (fig. 2.7a). FDTS molecules react covalently on oxide surfaces with their trichlorosilane (-$SiCl_3$) groups, with release of hydrochloric acid (HCl) (fig. 2.7b).

The major potential of this silane lies on its heavily fluorinated tail group which reduces surface energy. It's easily understood that FDTS is a more complex silane than HMDS. If the reaction between the FDTS molecules and the surface occurs, it is not guaranteed that all trichlorosilane groups react, which can lead to a horizontal conformation of the molecules (fig. 2.7c1,c2), with exposure of difluoromethylene (-CF_2) groups.

On the other and, if a vertical orientation of the molecule is obtained, a more close-packed self-assembled monolayer is achieved (fig. 2.7c3), leading to the exposure of trifluoromethyl (-CF_3) groups, which have higher hydrophobic potential [36]. The type and number of exposed groups consequent of molecule orientation highly influences the wettability of the surface.

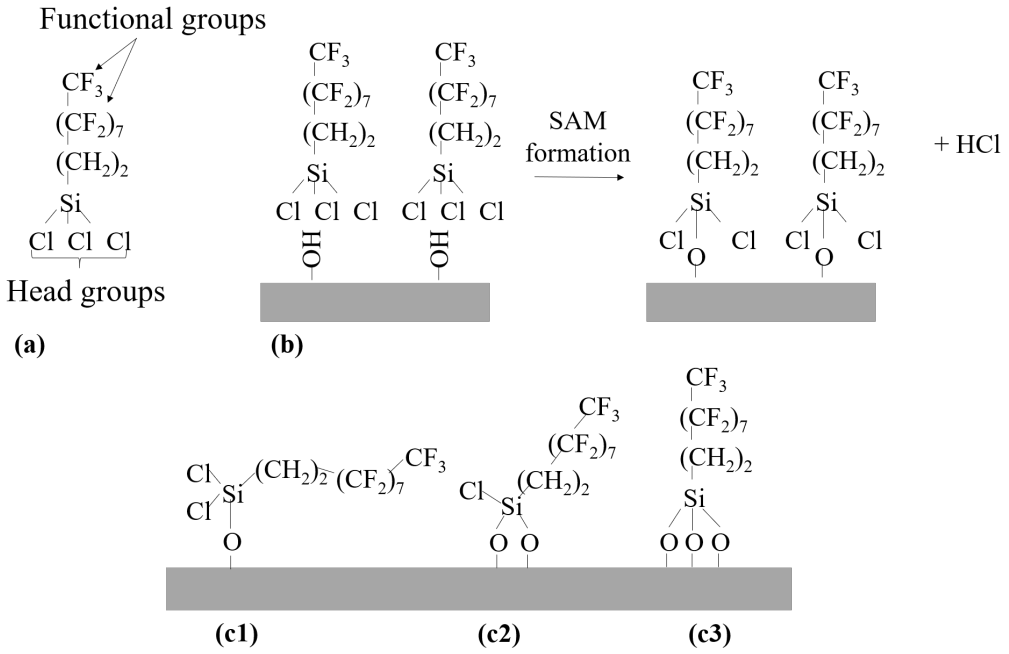

Figure 2.7: Scheme of **(a)** a FDTS molecule with trichlorosilane moieties as the head groups and fluorinated moieties as the functional groups, **(b)** the reaction of FDTS molecules with oxidized surfaces and **(c)** the several molecule orientations possible for FDTS: **(c1)** and **c2** represent a horizontal orientation and **c3** shows a vertical orientation (adapted from Silverio, V. *et al*, 2019).

In the field of cell biology, the hydrophobic character of surfaces may be useful for the study of cell behaviour and structural response, but not always the materials present such features and need modification. Shuai, H. and co-workers [37] developed chemically and physically modified chitosan membranes to probe cellular behaviors and molecular-level structural responses of NIH-3T3 fibroblasts (normal cells) ans *Ha-ras*-transformed cells (abnormal cells) that adhered onto the modified membranes. For this, the authors developed several membranes: FDTS-grafted, oxygen plasma-treated, nanotextured and pristine chitosan membranes (control samples). FDTS-grafted chitosan membranes showed an increase of contact angle from 87.3° to 127.3°, turning chitosan hydrophobic. With chemical modification, the authors observed that both NIH-3T3 fibroblasts and *Ha-ras*-transformed cells showed distinct actin and cytoskeleton organizations when comparing to cultures on coverslips and pristine chitosan membranes. The presence of different functional groups on these two substrates was the cause for such behaviours.

2.2.2.C APTES

(3-aminopropyl) triethoxysilane (APTES) is an aminosilane with the chemical formula $NH_2(CH_2)_3Si(OCH_2CH_3)_3$ (fig.2.8a). The three ethoxy (-OCH_2CH_3) groups are usually hydrolyzed to form silanol (Si–OH) groups, releasing ethanol (OC_2H_6). Amines are known to be hygroscopic and therefore even with anhydrous solvents, trace amounts of water are adsorbed. Silanol groups formed by hydrolysis react with

hydroxyl groups of surfaces by condensation, forming Si-O linkage over the surface (fig. 2.8b). Thus, the substrate is covered by a layer of exposed amine groups [38].

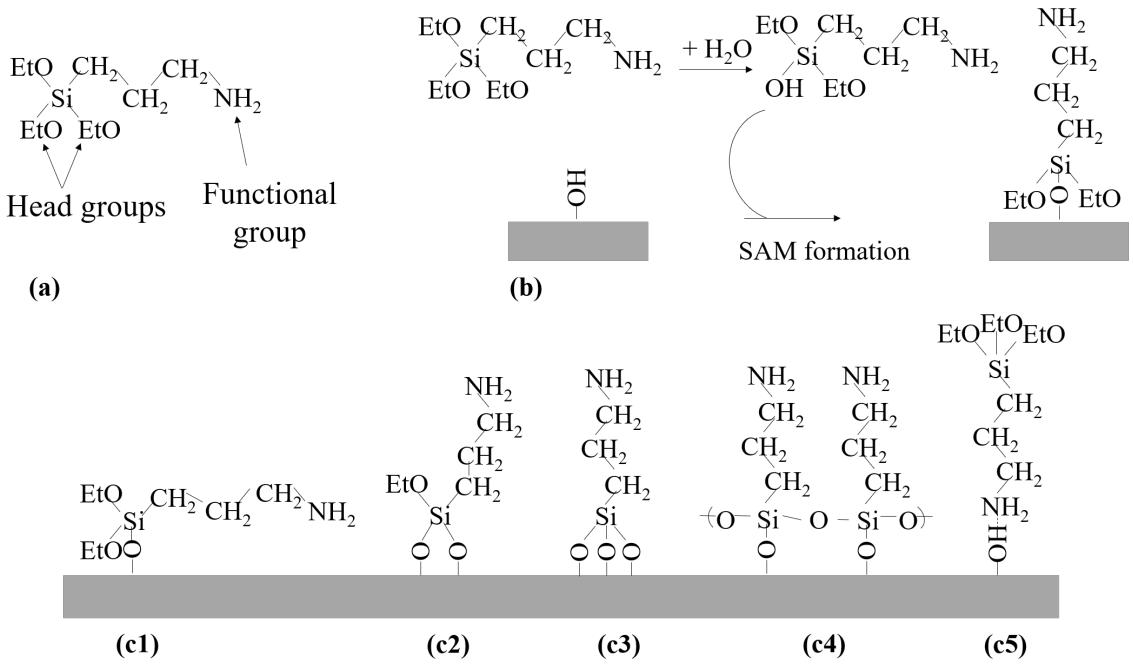

Figure 2.8: Illustration of **(a)** a APTES molecule with ethoxy groups (-OCH_2CH_3) as the head groups and a amine group (-NH_2 as the functional groups, **(b)** a generic reaction between APTES molecule and a hydroxyl-containing surface and the several molecule orientations for APTES: horizontal orientation from the reaction of one **(c1)** and two **(c2)** ethoxy groups and a vertical orientation consequent of the reaction of three ethoxy groups **(c3)**, cross-linking between APTES molecules **(c4)** or attachment of APTES molecules by hydrogen-bonds **(c5)** (adapted from Kyaw, H. *et al*, 2015).

Such as FDTS, the molecular orientation of APTES highly influences surface wettability. As shown in fig 2.8, the reaction between one (c1), two (c2) or three (c3) epoxy groups and the surface can occur, leading to different molecule orientations. The cross-linking between APTES molecules is also possible (c4) where silanol fragments, consequent of hydrolyzation, can react via condensation with neighboring silanol groups of other APTES molecules, producing siloxane bonds (Si-O-Si). Exposure of ethoxy groups can also be obtained (c5) if the amine group attaches to the surface by hydrogen bonding [39].

APTES is extensively employed for immobilization of DNA, antibodies, and enzymes. Kwon D. and co-workers [40] developed a facile colorimetric method for detecting residual penicillin G in milk using amine-immobilized glass vials and dendritic platinum nanoparticles. APTES was used to functionalize the interior of glass vials with amino groups, enabling the capture of penicillin G through the formation of amide bonds and consequent bonding of the penicillin G to the antibody-functionalized platinum nanoparticles.

Other applications are being studied for APTES, such as enhancement of surface biocompatibility in medical implants and drug delivery systems for humans. Sruthi S. *et al* [41] designed titanate nanotubes

(TiONts) as a drug delivery system across the brain. To deal with microglial activation and associated oxidative burst, the authors used APTES to chemically modify the TiONts surface (TiONts-APTES). Biocompatibility and interactions were studied *in vitro*, using murine microglial BV-2 cells. No morphological or plasma membrane permeability change was observed in cells exposed to TiONts-APTES. Exposure to the modified titanate nanotubes increased Reactive Oxygen Species (ROS) production and transient mitochondrial hyperpolarization, which normalized after 24h. However, there was no sign of microgial proliferation in BV-2 cells, evaluated by the cell cycle and cell count, suggesting no cell activation. Using this strategy of surface modification, the authors were able to create TiONts, at the same time more biocompatible and low in toxicity, more efficient for drug delivery in the brain.

2.2.3 Room Temperature Chemical Vapor Deposition (RT-CVD)

The two most relevant methods for surface silanization is liquid-phase and gas-phase silane deposition. The liquid approach or solution deposition is very simple and well documented in the literature. Basically, after adequate surface treatment, the substrates are submerged in a solution of silane, typically diluted in a strong solvent such as toluene, benzene with hexane, acetone, anhydrous ethanol, or a mixture of these [42]. The main disadvantage of the liquid-phase deposition is the usage of flammable and toxic organic solvents, which demand specialized handling. Furthermore, the chemical disposal process associated to this method can sometimes exceed the initial cost of the process, due to the usage of high volumes of organic reagents ($>$ 1 mL).

As for the gas-phase method, the substrates are exposed to a vapor-phase of the silane, usually formed under vacuum. Chemical Vapor Deposition (CVD) is one of the most used technique for silanization and requires a vacuum system, which can be somewhat expensive. Plus, most CVD processes are performed under high temperature conditions ($> 100°$). However, this technique requires no usage of organic solvents in the deposition and rinsing steps, showing to be a safer technique. Also, the amount of modifying agent needed is often less than a milliliter *per* run, so there is little to no waste disposal or environmental consequences. Finally, this technique enables silane deposition at high rates and without any transportation of impurities by the gas-phase to the surface [43]. RT-CVD benefits from all the mentioned advantages with the extra of the chemical processes being performed under ambient temperature, turning the technique of silanization more cost-effective and easier to implement.

In the next chapter, the experimental techniques applied for SWM (specifically Room Temperature CVD and implementation of deterministic roughness) of several substrates used in microfluidic devices, biomedical implants and BioMEMS are described in detail, along with the microfabrication techniques, contact angle measurement and assessment of surface chemistry (XPS).

3

Experimental Technique

Contents

Chemical and physical SWM techniques enable the tailor of adhesion forces, solving problems of unwanted biomolecule-surface or surface-surface attachment and cell behavior. Surface wettability may be altered by gas-phase processes (e.g. ultrasonic spray pyrolysis, CVD and atomic layer deposition), wet-chemical processes (e.g. layer-by-layer deposition, dynamic modification with surfactants and protein adsorption) [20] and physical process (e.g. addition of nanoparticles, plasma etching and femtolaser irradiation) [44, 45]. Silanization by RT-CVD brings the advantage of applying layers of silanes to surfaces with a simple and cost-effective system in substrates needed in biological and biomedical applications. Deterministic roughness allows the control of structure dimensions for SWM, being easily reproducible.

In this chapter, the experimental techniques used for SWM: silanization by RT-CVD and implementation of deterministic roughness are described in detail. Methods of microfabrication, film growth, contact angle evaluation and XPS analysis are also described.

3.1 SWM by Room Temperature Chemical Vapor Deposition (RT-CVD)

3.1.1 RT-CVD

RT-CVD is a method used to deposit thin layers of chemical agents onto surfaces, usually under vacuum and at room temperature. Small volumes of chemical agents ($<$ 1 mL) are vaporized due to the low pressure conditions, forming a saturated atmosphere. The vapor-phase molecules adsorb onto the substrate, by a variety of chemical interactions (e.g. covalent bonds, electrostatic interactions, hydrogen bonds). In this work, HMDS, FDTS and APTES silanes were employed in SWM by RT-CVD, due to their hydrophobic potential and wide utilization in biological and biomedical fields. Substrates commonly used in microfluidics (silicon, glass, PDMS elastomer and SU-8 photoresist), thermoplastics (PS, PMMA and PET) and thin films (of gold, alumina and silicon dioxide) were exposed to volumes of 6 μL of HMDS, FDTS or APTES vapor on a vacuum desiccator (Bel-Art Products, fig. 3.1) for 2, 10, 20, 30 and 50 minutes at ambient temperature (22 °C) and pressure -0.78 $\pm$ 0.09 atm (R5 rotary vane vacuum pump, Busch).

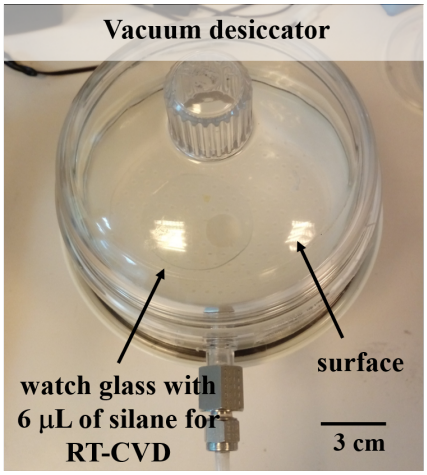

Figure 3.1: Vacuum system used for RT-CVD technique.

3.1.2 Materials Commonly used in Microfluidics

Hard flat samples of silicon (single side polished Si, mechanical grade, 0.65 mm thick, (100), University Wafer, fig. 3.2a), **glass** (76 x 26 x 1 mm thick, microscope slides, Normax, fig. 3.2b), **SU-8 2005** photoresist coatings (5 μm thickness, permanent epoxy negative photoresist, Microchem, fig. 3.2c) and **PDMS membranes** (10:1, 0.5 mm thickness, SYLGARD® 184 silicone elastomer, Dow Corning, fig. 3.2d) were exposed to HMDS vapor (hexamethyldisilazane ($HN[Si(CH\_3)_3]_2$, 161.40 $gmol^{-1}$, 96.0 % , TCI) and FDTS vapor (perfluorodecyltrichlorosilane, $(CF_3(CF_2)_7(CH_2)_2[SiCl_3]$, 581.56 $gmol^{-1}$, 97.0 %, Alfa Aesar) by RT-CVD.

Silicon samples (University Wafer) and **glass** (Normax) were previously washed with Alconox® anionic detergent for 3 hours, rinsed with isopropanol ($> 99.8\ \%$, Labchem), DI water and blow dried. **PDMS** membranes (SYLGARD® 184 silicone elastomer, Dow Corning) were fabricated by mixing 3 dimethyl siloxane and 184 silicone elastomer (cross linking agent) in a ratio of 10:1 and put on a vacuum desiccator for 1 hour (1-800-4Bel-Art, Bel-Art Products) to remove any bubbles formed during the mixing step. Finally, a cure step was performed at 70 °C for 1 hour (Memmert GmbH + Co. KG 100-800 oven). A homogeneous coating of **SU-8 2005** of 5 μm thick was obtained on silicon pieces previously dehydrated, by a 2-step spin coating process (step 1: 500 rpm for 10 s at 100 $rpm.s^{-1}$, step 2: 3056 rpm for 30 s at 300 $rpm.s^{-1}$; Modular spin coater ws-650-23NPP, Laurell Technologies Inc.) followed by a soft baking step on a hot plate (95 °C for 2 min, SD160 hotplate, Stuart). Later, a step of UV light exposure (17 s, 5.95 $W.cm^{-2}$, UH-H 254, UV Light Technology LTD; black filter: 320-405 nm) of the SU-8 2005 was performed, followed by a second soft bake step (95 °C for 3 min). Finally, the substrate was left to cool down to room temperature ($\sim$ 22°C). To avoid any surface contamination, all steps were executed inside a laminar flow hood (Faster-BSC-EN).

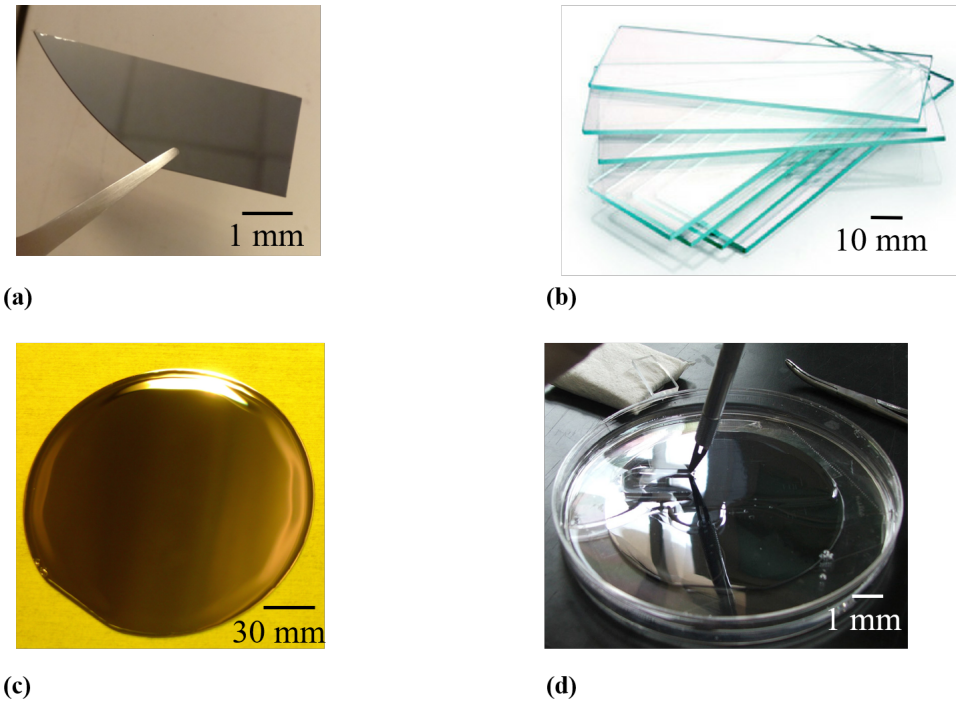

Figure 3.2: **(a)** Silicon and **(b)** glass samples used for RT-CVD. **(c)** SU-8 substrates and **(d)** PDMS membranes 0.5 mm thick were individualized after microfabrication.

3.1.3 Thermoplastics

PET (polyethylene terephthalate, 65 x 25 mm, 0.107 mm thick, Adhesives Research, fig. 3.3a), **PS** (polystyrene, 15 x 15 mm, 3 mm thick, CRYLUX®, fig. 3.3b) and **PMMA** (poly(methyl methacrylate), 20 x 20 mm, 1.5 mm thick, Perspex®, fig. 3.3c) samples were exposed HMDS, FDTS and APTES vapor ((3-aminopropyl)triethoxysilane, $NH_2(CH_2)_3Si(OCH_2CH_3)_3$, 221.37 $gmol^{-1}$, 99.0 %, Acros Organics), by RT-CVD.

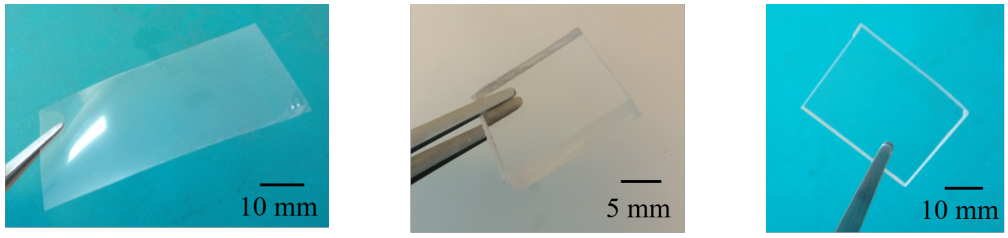

Figure 3.3: Samples of **(a)** PET, **(b)** PS and **(c)** PMMA thermoplastics submitted to RT-CVD.

PS (CRYLUX®) and **PMMA** (Perspex®) samples were rinsed with isopropanol, DI water and blow dried. **PET** samples (Adhesives Research) were washed with Alconox® anionic detergent for 1h at room

temperature ($\sim$ 22°) and then rinsed with IPA, DI water and carefully blow dried. The substrates were stored in Petri dishes at ambient conditions until SWM assays.

3.1.4 Thin Films

Thin films of **gold** (18 x 10 mm, 500 Åthick, fig. 3.4a), **silicon dioxide** (25.4 x 25.4 mm, 1000 Å thick, fig. 3.4b) and **alumina** (22 x 12 mm, 1000 Å thick, fig. 3.4c) pieces were exposed HMDS, FDTS and APTES vapor ((3-aminopropyl)triethoxysilane, $NH_2(CH_2)_3Si(OCH_2CH_3)_3$, 221.37 gmol^{-1}, 99.0 %, Acros Organics), by RT-CVD.

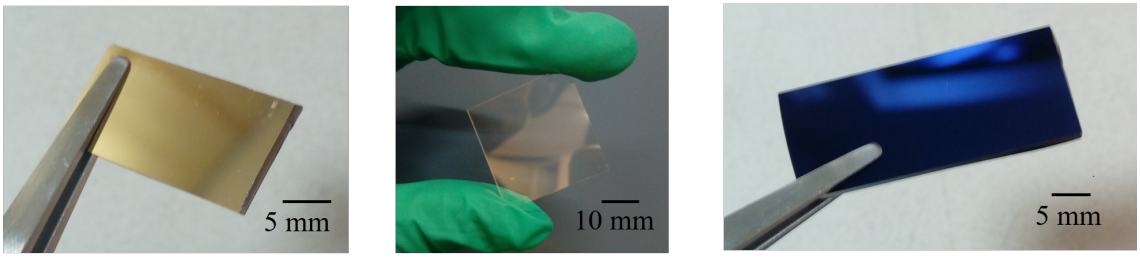

Figure 3.4: Thin films of **(a)** gold, **(b)** silicon dioxide and **(c)** alumina submitted to RT-CVD.

Gold thin films of 500 Å were deposited on silicon surfaces by Ion Beam Deposition and stored in petri dishes under ambient conditions. Due to the poor adhesion of gold to silicon surfaces, a prior deposition of a chromium thin film is necessary (fig. 3.5a, Alcatel, base pressure of 7.0x10^{-7} torr, Cr: 2.89 mtorr, 20 sccm, 20 W_{RF}; Au: 2.89 mtorr, 20 sccm, 20W_{RF}, 9 W, 160 Vbias) For surface wettability assays, gold thin film pieces were rinsed with isopropanol ($>$ 99.8 $\%$, Labchem), DI water and blow dried.

Aluminum oxide thin films with a thickness of 1000 Å were deposited onto silicon surfaces by Radio Frequency Sputtering (fig. 3.5b, UHV II, base pressure of 7.5x10^{-7} torr, applied power of 200 W_{rf}, 543 Hz, argon flux of 43.9 sccm, deposition pressure of 4.6 mtorr). These films were used for SWM assays immediately after deposition, so no cleaning step was performed.

Silicon dioxide thin films of 1000 Å were grown on glass surfaces (Corning® Eagle XG®, 0.7 mm thick) by Magnetron Sputtering (fig. 3.5a, Alcatel, applied power 140W_{RF}, argon flux of 20 sccm, 4 rpm, deposition pressure of 1.80 mTorr, base pressure in the order of 10^{-7} torr, deposition rate of 0.44 Å/s) and stored in petri dishes under ambient conditions, until SWM assays.

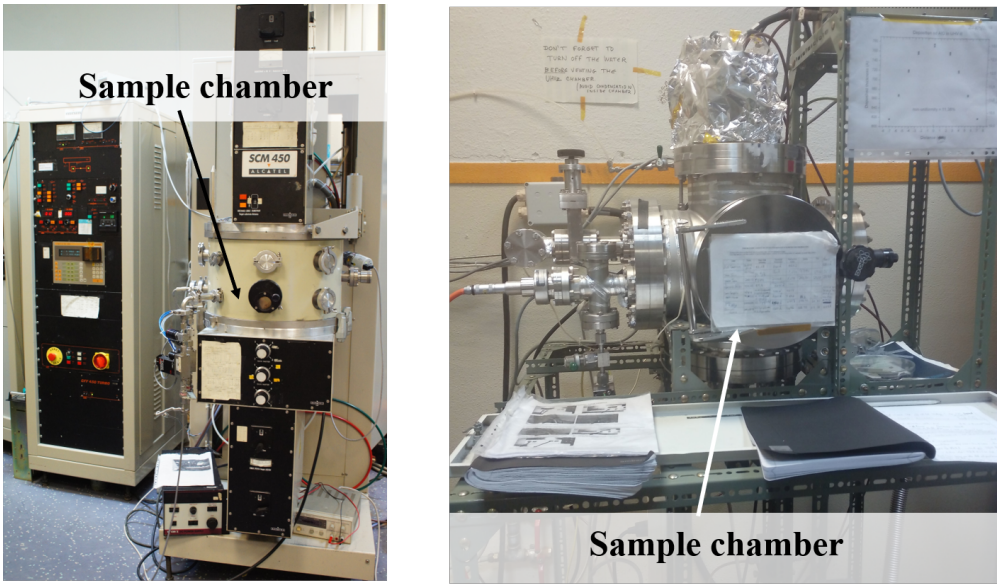

Figure 3.5: (a) Alcatel and **(b)** UHV-II apparatus for deposition of thin films of gold, silicon dioxide and alumina.

3.2 SWM by Deterministic Roughness

Physical methods to change surface wettability rely often on the growth or removal of material from the surface. In this study, surfaces of silicon with patterned SiO_2 film were prepared to study the influence of the size and spacing of thin film elements in surface wettability tailoring.

Many biological and biomedical applications make usage of silicon dioxide thin films, due to its many advantages, such as biocompatibility and easy processability. The application of photolitography techniques for the implementation of deterministic roughness is opening new ways to study cell attachment and growth rate consequent of surface topography [46]. Studies regarding cell patterning find many applications such as drug discovery and tissue engineering [47, 48]. Wettability assays on surfaces with deterministic roughness help researchers understand how the wettability consequent of roughness correlates to specific cells and enzymes. It is well known that cells and enzymes have a high affinity to hydrophobic surfaces but the behavior of these biological components is more complex than that. Different types of cells react differently to various surface topographies and the comprehension of these behaviors is of high interest in academic research, as to understand how to control the response of cells (e.g. migration, proliferation, adhesion and cell-to-cell communication) to certain drug delivery systems or cell culture materials.

Deterministic roughness can be obtained by controlling three structure variables that influence the

behavior of a liquid droplet on the surface: structure size, spacing and height. To evaluate the impact of spacing and structure size in surface wettability, square patterns were created by photolithography on silicon dioxide thin films. Structure size varied between 1 to 5 μm, while spacing between the structures varied between 2 and 5 μm, with a fixed height of 915,8 Å. The fabrication process was as follows: silicon substrates (single side polished Si, mechanical grade, 0.65 mm thick, (100), University Wafer) were washed with acetone (100 $\%$, Labchem), rinsed with isopropanol ($>$ 99.8 $\%$, Labchem), deionised water and blow dried. A 1000 Å thin film of silicon dioxide was deposited onto silicon surfaces by Magnetron Sputtering (fig. 3.5, Alcatel, B.P of 9.8x10^{-7} torr, 1.80 wt, applied power of 140 w$_{rf}$, 4 rpm).

Square structures of varying size (*L*) and spacing (*d*) were designed in AutoCAD (fig. 3.6) and microfabricated on the thin films of silicon dioxide, by a photolitography process (fig. 3.7a,b) which includes four steps: 1) substrate pre-treatment (described in anex A), 2) coating of the surface with a 1.5 μm thick layer of positive photoresist PFR 7790G27cP (JSR Micro, spread step at 500 rpm for 10 s, followed by a spin coating at 2500 rpm for 30 sec and a soft bake step at 87 °C for 60 sec), 3) exposure to UV light (energy: 55% , power: 100 mW, focus: -10, Heidelberg Instruments Direct Laser Lithography System) and 4) photoresist development (baking step at 110 °C for 60 sec, followed by a cooling step for 30 sec and exposure to photoresist developer TMA238WA (JSR Micro, for 60 sec).

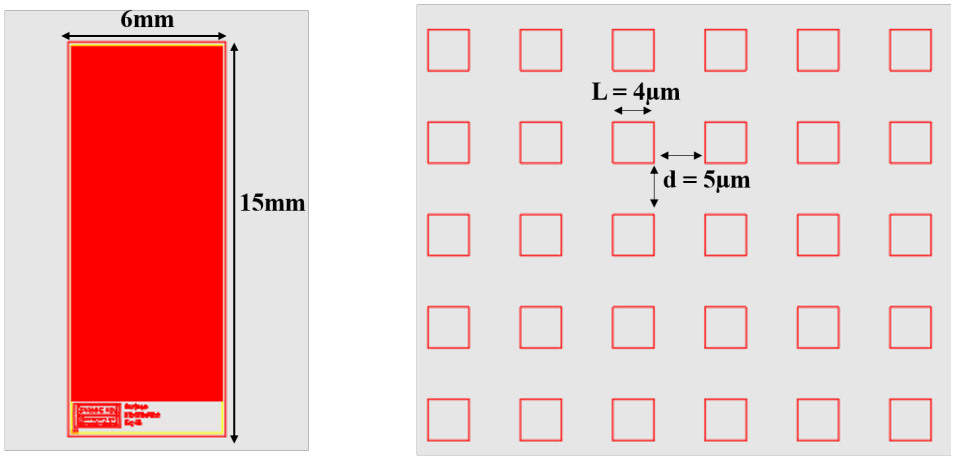

Figure 3.6: (a) Example of the design of a 6 x 15 mm sample in AutoCad with **(b)** 4x4 μm squares spaced by 5 μm.

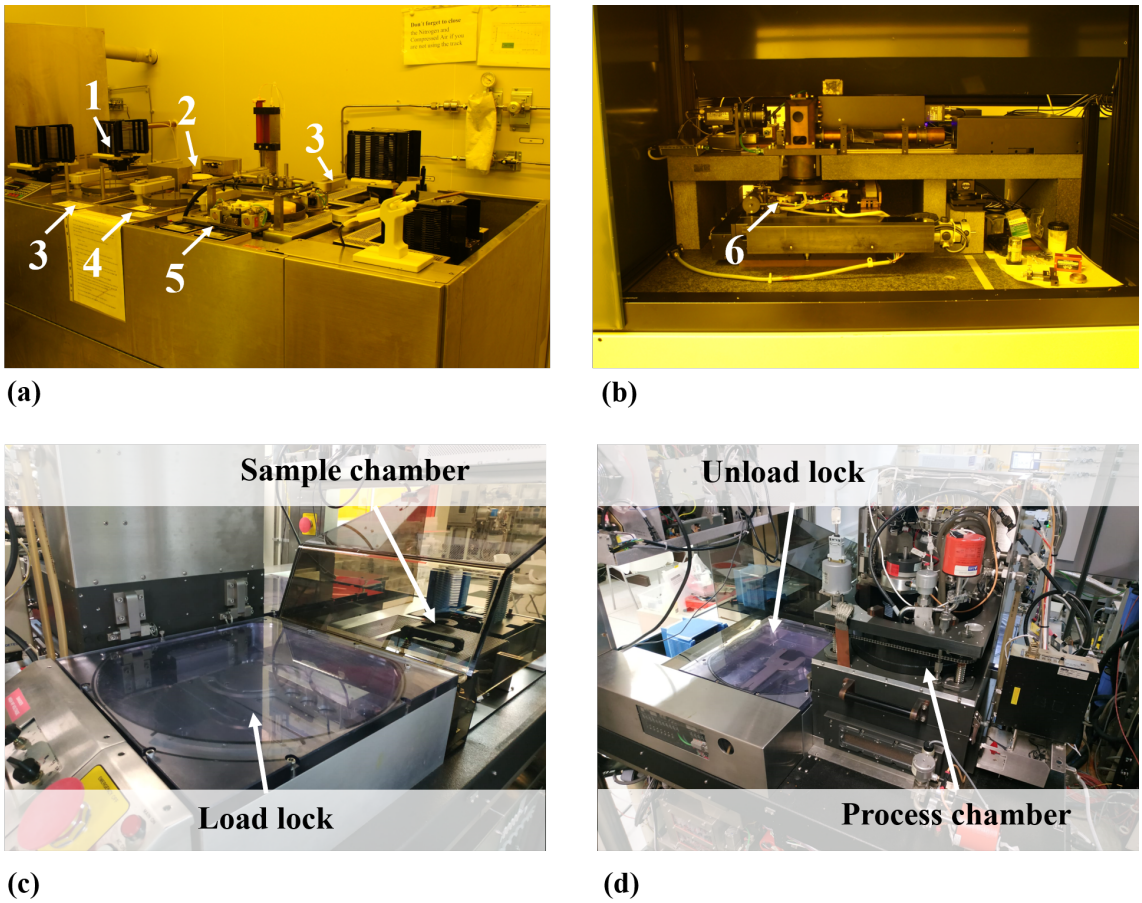

Figure 3.7: The first two pictures presents the photolitography machinery: where **(a)** shows the tracks for photoresist deposition (1 - sample holder, 2 - PR deposition,3 - soft bake step) and development (4 - platform for sample cooling, 5 - exposure to developer solution) and **(b)** the Direct Laser Lithography System (6 - platform for exposure of sample to UV light). The pictures below display the Reactive ion etching system where **(c)** presents the load zone of the samples and **(d)** shows the CF_4 plasma chamber and unload zone of etched samples.

After the definition of the structures on the PR, an etching step by reactive ion etching of the exposed silicon dioxide was performed with tetrafluoromethane (CF_4) (fig. 3.7c,d), LAM Research 4500, applied power of 100 W, 100 sccm CF_4, 200 sccm water, base pressure of 140 mTorr, etching rate of 9.1585 Å.s^{-1}).

The etched silicon dioxide thin films were individualized (Disco Dad-321 Dicing Saw) into 6 x 15 mm pieces, were each square pattern was present (fig. 3.8).

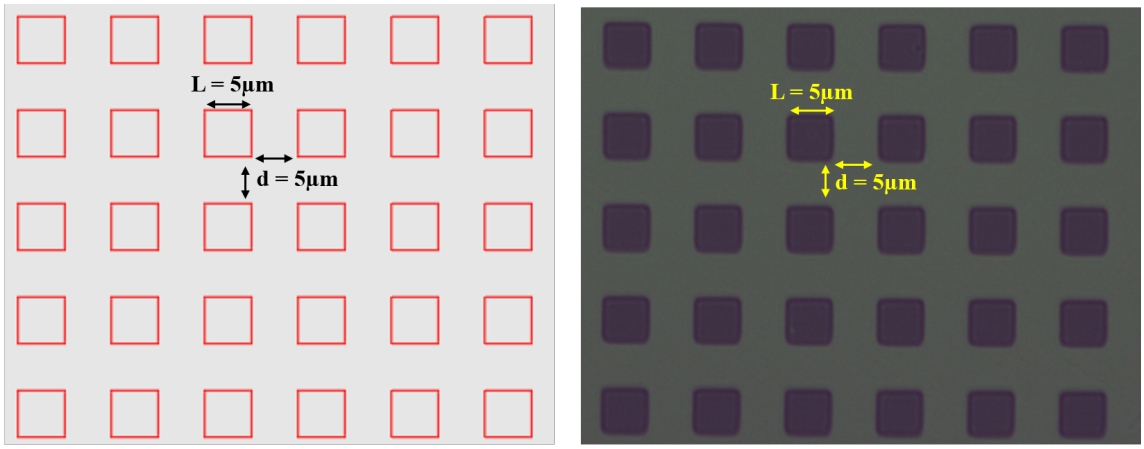

Figure 3.8: (a) Design of 5 x 5 μm squares with 5 μm spacing in AutoCad and **(b)** respective structures obtained in SiO_2 films (50 x amplification).

Finally, a resist stripping process was followed, were the silicon dioxide pieces were immersed in Microstrip 3001 (Fujifilm) for 1 hour in a thermostatic ultrasounds bath at 65 °C. The substrates were then rinsed with isopropanol, deionised water and blow dried with compressed air.

3.3 Contact angle evaluation

Measurement of contact angle of static droplets is a practical method to evaluate the wettable behaviour of a given surface. The contact angle, defined as the internal angle between a liquid drop and a solid surface, is consequence of surface tension phenomena, adhesion (liquid-surface) and cohesion (liquid-liquid) forces. If the adhesion forces exceed the cohesion forces, the surface shows a high wettability or high surface energy ($\theta < 90°$), while if the cohesion forces surpass the adhesion forces, a low wettability or low surface energy is observed ($\theta > 90°$).

For contact angle evaluation, a controllable syringe pump (NE 4000, New Era) with a 1 mL syringe (CODAN) and polyethylene tubbing BTPE-90 (863.3 μm inner diameter, Instech Lab) were used to dispense droplets of Deionised (DI) water and PBS solution onto the surfaces (fig. 3.9): 6 μL droplets for Si, glass, PDMS elastomer and SU-8 2005 photoresist; 3 μL drops for thermoplastics and thin films.

Endurance of silanization with HMDS and FDTS on silicon surfaces was also analyzed, through CA measurements over 65 hours, after 50 min of RT-CVD. Wettability of structured surfaces was assessed with CA measurements of 3 μL droplets of DI water. Control measurements of CA (CA_{t0}, $CA_{L=0}$ and $CA_{d=0}$) were also performed in clean, unmodified surfaces. The different combinations of experimental conditions (surface - liquid - chemical agent - exposure time) were repeated three times. For drop dispense, the substrates were placed in a control chamber, to reduce surface contamination. Pictures

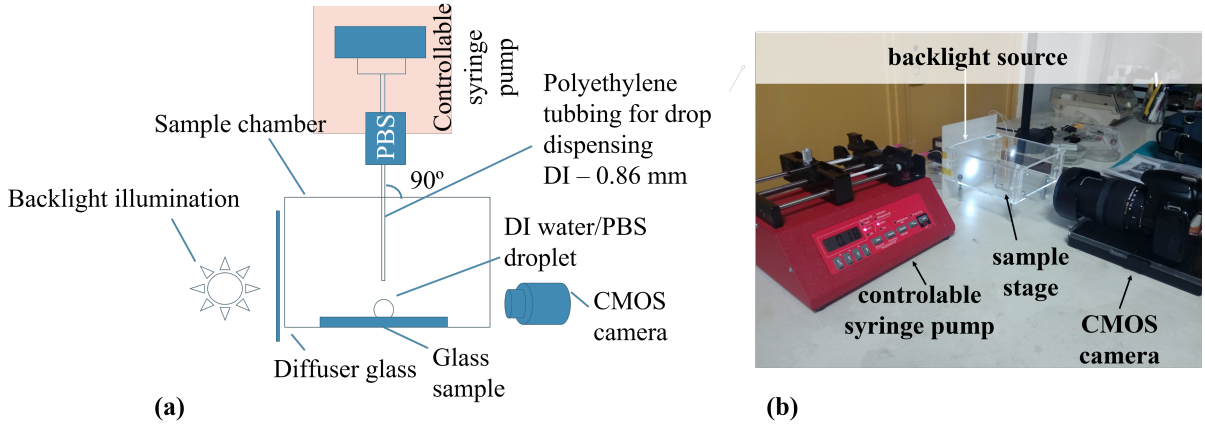

Figure 3.9: (a) Scheme of the system used for CA measurements of the several substrates after chemical and physical SWM. **(b)** System used for CA evaluation.

of droplets were taken with a CMOS camera (5.1 µm pixel size, 12 Mpixel) coupling a macro lens with 0.33 maximum magnification, for CA analysis. A light source was placed behind the control chamber, to ensure high contrast in the pictures. Pictures of droplets on surfaces chemically functionalized were recorded under ambient conditions within 5 min after RT-CVD exposure. CA analysis was performed using Image J software with LBADSA plugin (fig. 3.10), created by Stalder and co-workers [49].

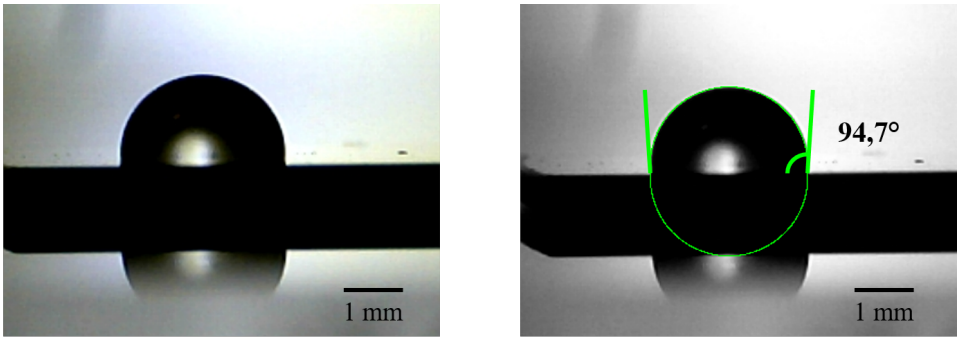

Figure 3.10: (a) Droplet of DI water on alumina thin film after RT-CVD with FDTS for 20 min and **(b)** measurement of CA using Image J LB-ADSA software.

LBADSA plugin returns the CA using the best solution for the Young-Laplace equation (3.1) where γ is the surface tension, R_1 and R_2 are the principal radii of curvature at any point on the drop and ΔP is the pressure difference across the surface.

$$\Delta P = \gamma(\frac{1}{R_1}) + (\frac{1}{R_2}) \tag{3.1}$$

In this software, the user must define the shape of the droplet by controlling six variants: *c*, capillary

constant (water: 134,753 m^{-2}), *x*, *y*, *h*, *d* and *b*, all dimensional parameters.

3.4 X-ray Photoelectron Spectroscopy

The surface composition was also evaluated by X-ray photoelectron spectroscopy (XPS). XPS, also known as Electron Spectroscopy for Chemical Analysis (ESCA), is a technique used to identify the chemical composition of a given surface layer, making use of Einstein's photoelectric law. Einstein's photoelectric law states that when a photon hits a surface with sufficient energy, it will transfer the energy to an atom present on the surface, leading to the removal of an electron (fig. 3.11).

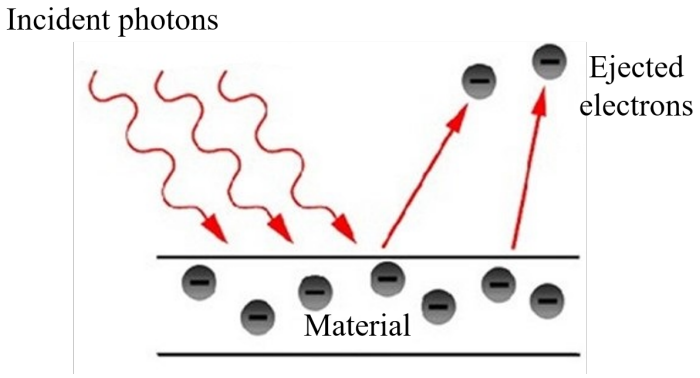

Figure 3.11: Scheme of Einstein's photoelectric effect.

This electron will acquire kinetic energy that is equal to the energy of the photon that hits the surface minus the binding energy (BE) of the electron to the atom. This relation is presented in equation 3.4:

$$E_{kinetic} = h\nu - E_{binding}$$

where $E_{kinetic}$ represents the kinetic energy acquired by the electron, $h\nu$ is the energy of the X-ray photons and $E_{binding}$ the energy that binds the electron to the atom.

Each pair of electrons (with opposite spin numbers) of a given atom occupy a certain orbital, with a discrete level of energy. The orbital will experience different electrostatic attraction depending on the atom since the attraction will be different for each atomic nucleus. In order to determine the atom present at a given surface, XPS relies on the binding energy of core electrons, which are like a signature of the element present, thus providing the composition of the surface plus the chemical and electronic state of the elements within the surface. Since core electrons are very hard to remove, due to the high attraction felt by the nucleus, highly energetic protons are required (X-ray energy). All elements can be identified using the core electron binding energies with the exception of hydrogen and helium, since

these elements have no core electrons [50].

XPS spectra is obtained by irradiating a solid surface with a beam of X-rays while simultaneously measuring the kinetic energy and electrons that are emitted from the top 1-10 nm layer of the material being analyzed. Peaks in the spectrum appear when electrons of a particular energy are emitted from the surface, which enable the calculation of the binding energy of the electron ($E_{binding}$, eq. 3.4) and consequently, the identification and quantification of the atom from which the electron was released.

The elemental analysis of clean, non-exposed sample surfaces and modified surfaces was performed in Kratos XSAM800 apparatus (fig.3.12) with Mg Kα radiation (hν = 1253.6 eV).

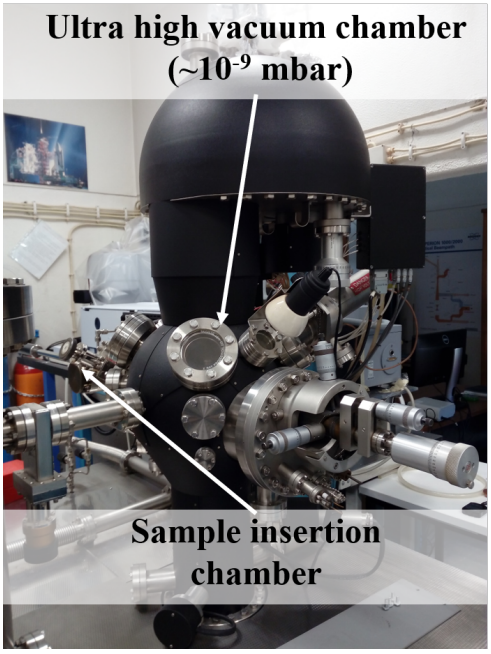

Figure 3.12: X-ray Photoelectron Spectroscopy (XPS) apparatus for analysis of surface chemistry.

Spectrometer operation conditions, take-off angle (TOA), pressure and temperature of analysis were as described in Ferreira *et al* [51]. Spectra (with a step of 0.1 eV) were collected by the software Vision 2 for Windows, Version 2.2.9 from Kratos. Data processing was performed using the freeware XPSPeak 4.1. Shirley backgrounds and Gaussian-Lorentzian products were used for curve fitting. No flood gun was used for neutralizing charge accumulation. The shift due to charge accumulation was corrected using as reference the BE of aliphatic C 1s photoelectrons set to 285 eV [52, 53]. For quantification purposes, the sensivity factors (SF) used were those furnished by the equipment library: 0.318 for C 1s, 0.736 for O 1s, 0.505 for N 1s, 0.371 for Si 2p, and 0.257 for Al 2p. The measurements were conducted at Centro de Química-Física Molecular (CQFM), of Instituto Superior Técnico.

4

Results and Discussion

Contents

In this chapter, results consequent of chemical functionalization and topography modification are discussed. Silanization by RT-CVD was employed in: substrates commonly used in microfluidics (Si, glass, PDMS and SU-8 photoresist), thin films (of gold, alumina and silicon dioxide) and thermoplastics (PET, PS and PMMA). The type of groups exposed at these substrates, the chemical agent used and CA value of the untreated surfaces are presented in table 4.1. Deterministic roughness was employed for SWM of silicon dioxide thin films, where square structures of varying size and spacing were designed by a photolitography process. Variables such as time and chemical functionalization agent, material of the surface and consequently functional groups at the surface and deterministic surface roughness elements present and their influence on SWM is evaluated.

Table 4.1: Substrates submitted to silanization by RT-CVD with specific chemical agents. The exposed groups of the untreated surfaces and initial contact angle are also presented. * Surfaces may present carbonaceous contamination.

Family	Surface Material	Groups exposed at the surface	CA_{t0}	RT-CVD agent
Commonly used materials in microfluidics	Silicon	-OH	17°	HMDS, FDTS
	Glass			
	SU-8	$-OCH_2CR$	120°	
	PDMS	$-CH_3$	108°	
Thermoplastics	PET	=O	74°	HMDS, FDTS, APTES
	PS	$-C_6H_5$	84°	
	PMMA	=O, $-OCH_3$	67°	
Thin films	Silicon dioxide	-OH*	80°	HMDS, FDTS, APTES
	Alumina	-OH	16°	
	Gold	-*	80°	

4.1 Surface material: silicon, glass, PDMS and SU-8

Silicon, glass and polymer-based materials, such as PDMS and SU-8 photoresist, are common substrates used in microfabrication and microfluidic devices. The usage of these materials in biological and biomedical fields may require the tailor of surface wettability to avoid biofouling, to increase the affinity between the surface and nanoparticles (necessary for biological detection) or to study the effects of hydrophobic/hydrophilic conditions in cell morphology and cell behaviour. Prior to the biological application is the microfabrication of the device, which can also benefit from chemical SWM to weaken unwanted adhesion forces between substrates. Next, results obtained of chemical exposure of samples of silicon, glass, PDMS and SU-8 PR to HMDS and FDTS silanes by RT-CVD are discussed.

4.1.1 HMDS Chemical Vapor Deposition

Results presented in figure 4.1 show that CA on silicon and glass (both hydroxyl-containing surfaces), initially hydrophilic (CA $\cong$ 17°) showed an increase after exposure of the surfaces to HMDS vapor

molecules, which indicates a decrease in surface interfacial energy. Surface coverage with a SAM of HMDS molecules reaches a plateau after 30 min of CVD exposure (CA $_{glass}$ = 65° and CA $_{Si}$ = 73°).

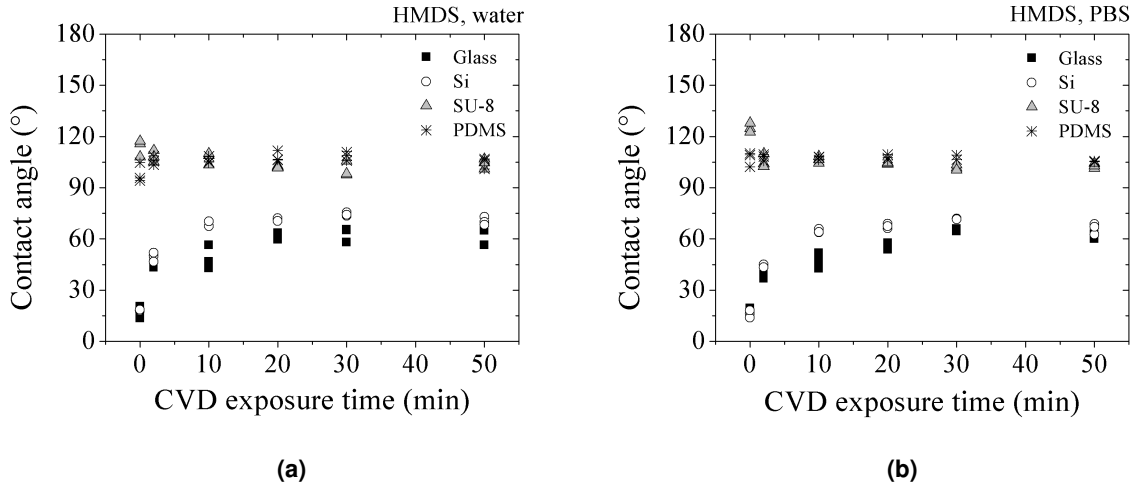

Figure 4.1: Contact angle of **(a)** DI water droplets and **(b)** PBS droplets on rigid surfaces of glass, silicon, SU-8 and PDMS after RT-CVD with HMDS.

As mentioned in chapter 2, trimethylsilanol (-Si[CH_3]$_3$) groups present in HMDS molecules react covalently with hydroxyl groups present on the silicon-based surface (fig. 4.2), establishing siloxane (Si-O-Si) bonds, with the release of ammonia (NH_3). When the reaction is complete, the surface is covered with methyl (-CH_3) groups, responsible for the decrease of surface energy due to their non-polar character. Besides the hydrophobic potential of the exposed groups at the surface, the surface interfacial energy is also dependent on the extent of surface coverage, unreacted residual groups from the silane on the surface, distribution and orientation of the functional groups grafted on the surface.

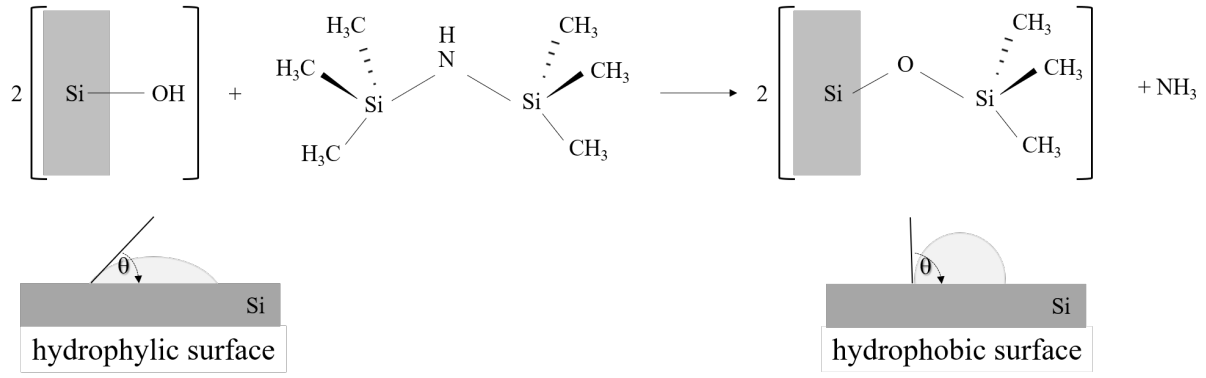

Figure 4.2: Reaction between HMDS molecules and hydroxyl-exposing surfaces. Trimethylsilanol groups of HMDS molecules react covalently with hydroxyl groups, releasing ammonia (adapted from Silverio, V. *et al*, 2019).

Measurements of CA for DI water and PBS drops on **SU-8** surfaces showed a decrease after ac-

tivation with HMDS (variation from $\simeq$ 120° to 100°) throughout the different exposure times, reaching a plateau after 10 min of activation. SU-8 derives its name from the presence of eight epoxy groups *per* molecule (fig. 4.3), which are responsible for the low wettability of the surface. The decrease of CA observed is believed to originate from a typical reaction between epoxide groups present in SU-8 molecules and a secondary amine, HMDS (fig. 4.4).

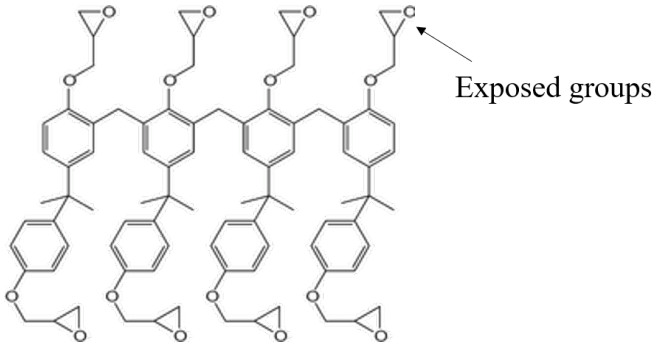

Figure 4.3: Chemical structure of one molecule of SU-8 photoresist (adapted from Genolet, G. *et al*, 1999).

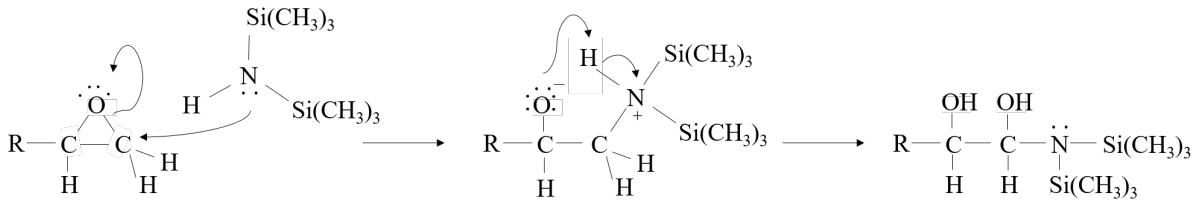

Figure 4.4: Reaction between HMDS molecules and epoxide groups of SU-8 molecules. The nitrogen free electrons react with the methylene group of the epoxide moieties, generating hydrophilic hydroxyl groups (adapted from Silverio, V. *et al*, 2019).

An attack by the nucleophile atom of HMDS (in this case, the nitrogen atom) occurs, where the free electrons of the amine react with the methylene group (-CH_2) present in the epoxy moiety, generating hydroxyl groups [20]. The presence of these groups in the molecules of SU-8 lead to an increase of hydrogen-bonds between the surface and polar liquids and therefore, an increase in liquid-surface adhesion forces, which translates into a decrease in CA values. However, the increased number of hydrogen-bonds are not sufficient to surpass the cohesive forces of the bulk water/aqueous droplet solution, thus the surface maintains a hydrophobic behavior (CA $\simeq$ 100°) [54].

Untreated **PDMS** substrates show an initial hydrophobic behaviour ($CA_{t0} \simeq$ 108 °), consequent of the exposure of methyl (-CH_3) groups on the surface (fig. 4.5). The chemical exposure of this substrate to HMDS vapor did not exhibit significant changes after chemical exposure.

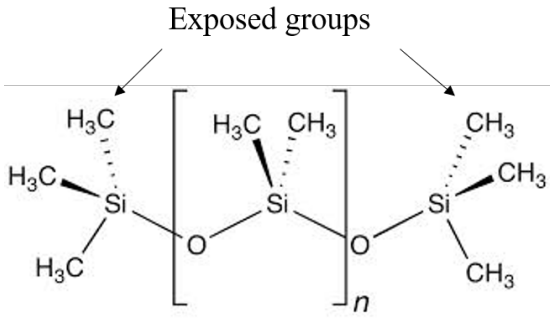

Figure 4.5: Molecular structure of PDMS elastomer, where *n* represents the number of repetitions of the monomer molecule (adapted from Silverio, V. *et al*, 2019).

It is well known that methyl groups decrease the interfacial energy of surfaces, as a result of their non-polar character [55]. Hence, surface-liquid interaction forces on surfaces containing methyl groups are expected to be weaker than those containing hydroxyl groups or hydrogen atoms. Also, reactiveness of methyl groups depends on the adjacent substitutes present in the molecule. In the case of PDMS, these groups are very nonreactive and the nucleophile attack from HMDS does not happen. Nonetheless, this strategy for wettability modification of PDMS surfaces can be employed to prevent adhesion between PMDS masters and PMDS molds, commonly used in microfabrication [56].

4.1.2 FDTS activation

The increase observed in CA measurements of DI water (fig. 4.6a) and PBS droplets (fig. 4.6b) for **glass** and **silicon** surfaces (from $\simeq 17°$ to $\simeq 70°$) after exposure to FDTS vapor is a consequence of the exposure of heavily fluorinated tails that incorporate the silane molecules.

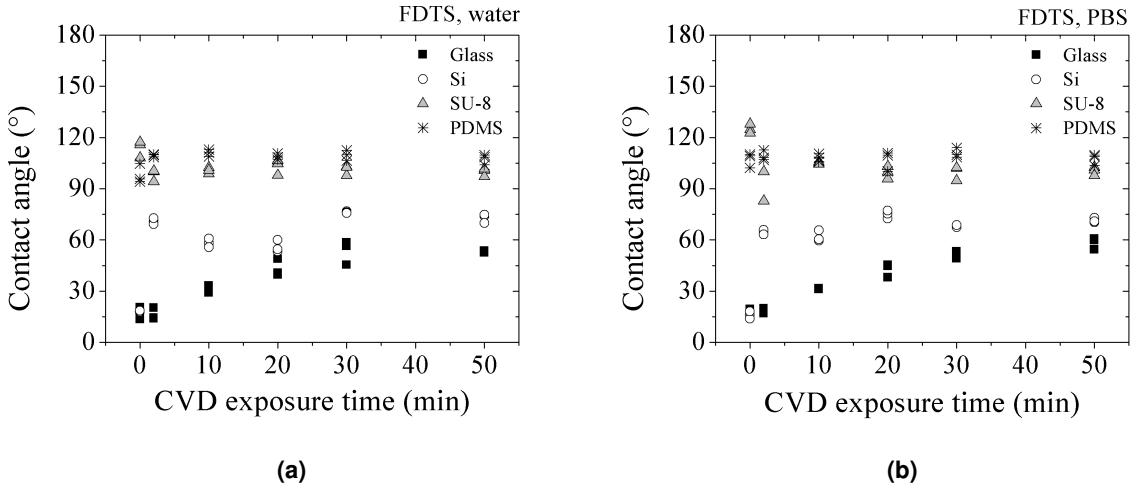

Figure 4.6: Contact angle of **(a)** DI water droplets and **(b)** PBS droplets on rigid surfaces of glass, silicon, SU-8 and PDMS after CVD using FDTS.

FDTS molecules form self-assembled monolayers (SAM) upon reaction with surfaces which expose layers of hydroxyl groups (fig. 4.7). Here, the Si atoms from the trichlorosilane groups (-$SiCl_3$) of FDTS covalently bond to oxide surfaces, releasing hydrochloric acid (HCl).

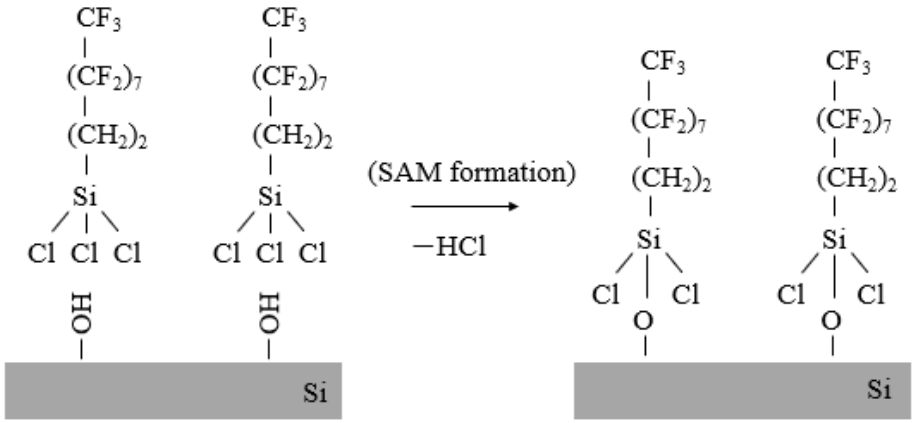

Figure 4.7: Reaction between FDTS molecules and an oxidized surface. Trichlorosilane groups of FDTS molecules covalently bond with oxygen atoms present at the surface, with release of hydrochloric acid (adapted from Silberzan, P *et al*, 1991).

The surface coverage with FDTS seems to be reached sooner for Si surfaces (saturation around 20 min of exposure to FDTS) then for glass surfaces (saturation around 50 min of exposure to FDTS). This behavior may be explained by the presence of boron ions in the composition of glass, which reduce the kinetics of FDTS with hydroxyl groups present at the surface [57].

Surfaces of **PDMS** exposed to FDTS showed a slight increase in CA values after 2 min of CVD with FDTS while SU-8 exposed surfaces suffered a slight decrease. As mentioned before, surface wettability modification is limited by the wettable character of the functional groups that attach covalently to the surface and the molecular orientation adopted by the whole molecule. Zisman [55] described the influence of hydrogen atoms on surface energy, by altering fluorocarbon surfaces (CF_3) with hydrogen atoms (CF_nH_{n-1}). The author observed increasing surface energy in the order: $CF_3 < CF_2H < CH_3 < CH_2$. The substitution of a single atom of fluorine for an atom of hydrogen doubled the surface energy, leading to an increase of surface wettability. Although no reaction occurs between PDMS surfaces and FDTS molecules, the presence of FDTS molecules onto the surface lead to the decrease of surface energy, due to the exposure of difluoromethylene (-CF_2) groups which, as explained in chapter 2, may derive from a horizontal orientation of the molecule.

Regarding **SU-8** substrates, the slight decrease in CA values might be explained by a chemical reaction that occurs in the polymerization phase of the PR. The polymerization of SU-8 monomers after post-exposure bake opens the epoxide group (fig. 4.8a), generating hydroxyl groups 4.8b) available to react with FDTS free molecules [58].

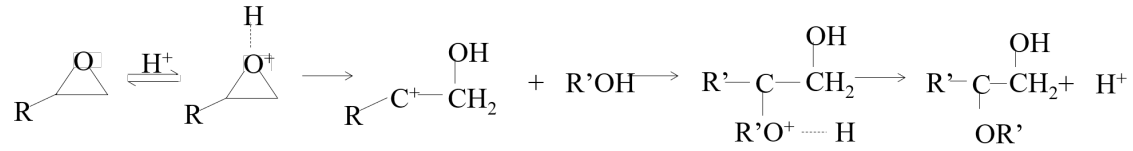

(a)

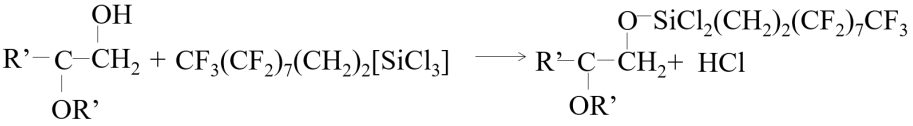

(b)

Figure 4.8: (a) Polimerization of SU-8 monomers in post-exposure bake. The formation of free hydroxyl groups on SU-8 surface enables the reaction of FDTS molecules, **(b)** leading to anchorage of fluorinated tails onto SU-8 surfaces (adapted from Silverio, V. *et al*, 2019).

4.1.3 Stability of self assembled monolayers of of HMDS and FDTS

The durability of silane formed self assembled monolayers (SAMs) is a crucial parameter for the application of chemical SWM to microfluidic devices for biological and biomedical applications. The stability of SAMs of HMDS and FDTS over time was evaluated, by exposing silicon surfaces to the silanes by RT-CVD for 50 minutes and measuring the CA for over 65 hours. The results displayed in fig. 4.9a) for DI water ($CA_{HMDS,water}$ = 63° ± 5°) and PBS solution ($CA_{HMDS,PBS}$ = 63° ± 4°) on silicon surfaces do not show significant variation of CA over time after 50 min of RT-CVD with HMDS whereas FDTS modified surfaces (fig. 4.9b) reveal a slight variability in CA over time ($CA_{FDTS,water}$ = 71° ± 9° and $CA_{FDTS,PBS}$ = 75° ± 6°).

This variability in surface contact angle may be a result of a lower-quality SAM on the surface consequent of the absence of a significant volume of water inside the desiccator. Although Si-Cl head groups of FDTS are strongly reactive with silanol (Si-OH) groups, it is improbable that all three functional groups of FDTS molecules react with the irregular OH groups present at the silicon surface. As a consequence, the FDTS SAM is constituted by molecules that are not bonded to the surface by covalent bonds, resulting in a low coverage or low-quality SAM [59]. To overcome this limitation, Zhuang and co-workers added water vapor to the reaction chamber to promote a prior hydrolysis reaction of the trichlorosilane groups of FDTS molecules which led to a denser and more stable FDTS SAM [60].

The chemical modification of silicon surfaces with HMDS and FDTS tested in this work is seen to be stable and persist for at least 65 hours (CA $\simeq$ 70°) after RT-CVD.

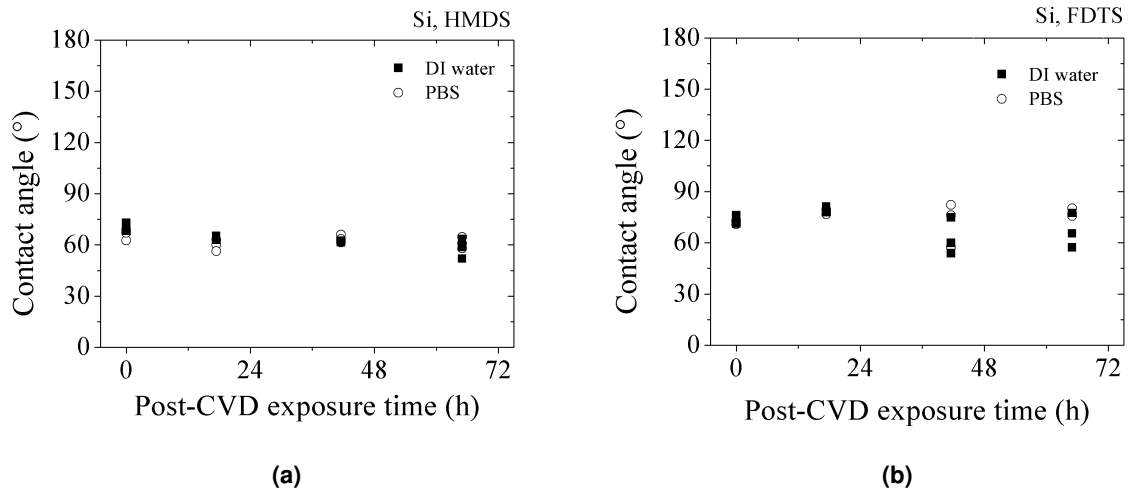

Figure 4.9: Variation of CA of DI water and PBS solution on silicon, after 50 min of exposure to **(a)** HMDS and **(b)** FDTS by CVD. For both scenarios, after 65 hours CA remains around 70°, which indicates a long-lasting effect of chemical activation of the surface.

4.2 Surface material: thermoplastics

Thermoplastics show a great potential of application in several fields, including microfluidics and biomedical implants. However, some concerns arise in the usage of these materials due to their hydrophobic behaviour, which can lead to medical complications and jeopardize biological detection. SWM of thermoplastics may be useful to increase thermoplastic-polymer adhesion forces in microfabrication or facilitate the fabrication of structures by replica moulding. Plus, phenomena such as biofouling may be reduced. Results regarding silanization of PET (polyethylene terephthalate), PMMA (poly(methyl methacrylate)) and PS (polystyrene) thermoplastics by exposure to HMDS, FDTS and APTES silanes by RT-CVD are presented below.

4.2.1 HMDS Results

Research regarding the impact of exposure of **PET** surfaces (hydrophobic material) to HMDS on surface wettability is very scarce and most address Radio-Frequency Glow Discharge (RFGD) as the deposition method. Kiaei et al [61] deposited ultrathin coatings of RFGD polymers of ethylene, tetrafluoro-ethylene and hexamethyldisiloxilane (HMDS) on PET substrates to verify the coatings' impact in platelet adhesion. Evaluation of the coverage of PET surfaces was performed, using measurements of DI water contact angles and ESCA spectrum analysis. PET surfaces covered with HMDS exhibited an increase in hydrophobic behavior (CA increased from 77° ± 2° to 99° ± 2°). ESCA spectrum revealed the presence of C-Si, C-C and C-H bonds, instead of C-O and O-C=O typically present in PET surfaces (fig. 4.10).

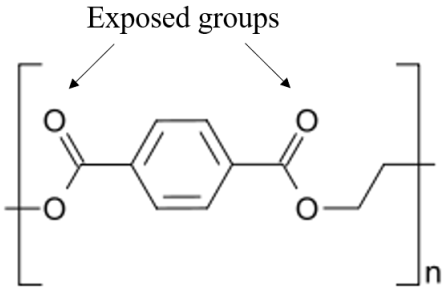

Figure 4.10: Molecular structure of PET thermoplastic, where *n* represents the number of repetitions of the monomer. PET molecules expose double-bonded oxygen atoms (adapted from Marchand-Brynaert, J., *et al*, 1995.

The latter result confirms the complete coverage of PET surfaces with HMDS molecules, which effect was observed by CA increase. However, ESCA data indicates that no reaction occurs between PET and HMDS molecules, as no change in chemical structure was detected. In this work, CA measurements of DI water and PBS droplets over RT-CVD modified PET surfaces did not evolve in significant value, being the initial CA value maintained even for the longest exposure time of 50 min ($CA_{PET} \simeq 74°$). Furthermore, results presented in fig. 4.11 show that measurements of CA for DI water droplets and PBS droplets in contact with PS and PMMA thermoplastics didn't alter significantly after chemical exposure to HMDS, as the CA measured for each pair solution-surface remained approximately the same ($CA_{PS} \simeq 84°$, $CA_{PMMA} \simeq 67°$), which may indicate that RT-CVD is not an adequate method to chemically modify thermoplastic surfaces with HMDS silane.

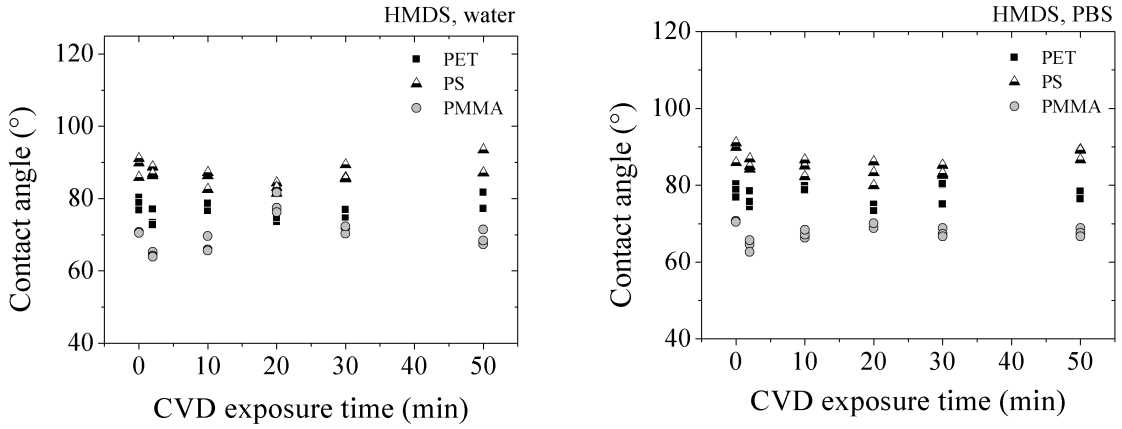

(a) **(b)**

Figure 4.11: Contact angle of **(a)** DI water droplets and **(b)** PBS droplets on rigid surfaces of PET, PS and PMMA thermoplastics after chemical exposure to HMDS by room temperature CVD.

Reaction between **PS** substrates and HMDS molecules is not expected, as the aromatic ring of

polystyrene is in a very stable configuration (fig. 4.12).

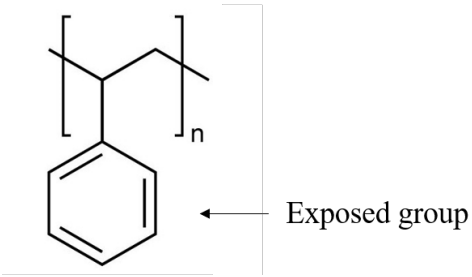

Figure 4.12: Molecular structure of PS thermoplastic, where *n* represents the monomer repetition and phenyl (C_6H_5OH) groups are exposed.

In this scenario, HMDS molecules would rest on top of PS surfaces after deposition. Since no alteration was observed in CA, it is possible that the hydrophobic potential of the whole HMDS molecules resembles the hydrophobic behavior of the polystyrene surface, since both are mostly constituted by hydrocarbon groups (-CH_n). Normally, functionalization of PS substrates is achieved with plasma treatments, where reactive plasma species induce the presence of polar groups on the surface, increasing the surface wettability [62]. Dowling, D *et al* [63] studied the effects of air plasma on the wettability of PS substrates, assessed by measurements of CA. The authors were able to increase the wettability of PS substrates (CA decreased from 83° to 64°), consequent of the presence of polar groups, such as C-O, C=O and -OH groups, at the surface. This results may indicate that a previous plasma treatment is necessary to chemically functionalize PS substrates with HMDS silanes, due to the high chemical affinity between hydroxyl groups and HMDS molecules. Although no significant modification on PS wettability was observed after exposure to HMDS, this method may be used to cover the substrate with a layer of HMDS and study the effects of methyl groups, present in a higher number than amine moieties, in cell behaviour [64, 65].

An ester group (RCOOR') can be observed in the chemical structure of **PMMA** (fig. 4.13), which is known to react with primary (RNH_2) and secondary amines (R_2NH, such as HMDS).

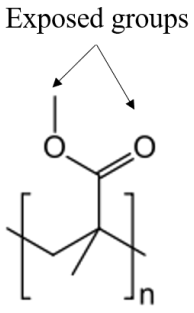

Figure 4.13: Molecular structure of PMMA thermoplastic, where *n* symbolyses the monomer repetition. PMMA exposes a double-bonded oxygen atom and a methoxy (-OCH_3) group.

However, this reaction can only occur in the presence of an alcohol, such as ethanol or methanol, at high temperatures [66] or in the presence of toluene [67]. Functionalization of PMMA substrates with HMDS may be implemented by more energetic methods for silane deposition, such as glow discharge plasma [68]. Another strategy to chemically functionalize PMMA substrates is the prior application of a UV/ozone step to originate hydroxyl groups on the surface, so that a covalent HMDS-surface reaction may occur. Yan and co-workers [69] studied the effect of HMDS treatment on polymer dielectric surface (one of them being PMMA substrates), untreated and treated with ultraviolet/ozone (UVO), for pentacene based organic thin film transistors (OTFTs). HMDS was deposited on PMMA substrates by RT-CVD for 2 hours. XPS analysis indicated that no reaction occurred between HMDS molecules and untreated PMMA surfaces, due to the absence of hydroxyl groups. The HMDS layer deposited connects to PMMA substrates by simple physical adsorption and could be removed with a cleaning process. A UVO treatment of PMMA surfaces increased the number of hydroxyl groups present at the surface, increasing surface energy (CA decreased from 83° to 30° after 300 sec of UVO exposure). Exposure of UVO-treated PMMA surfaces to HMDS lead to an increase in CA similar to the initial value of CA of untreated PMMA surfaces ($\simeq 75°$). Based in these conclusions, it is assumed that, although a negligible variation of CA values was observed after exposure of PMMA surfaces to HMDS silane by RT-CVD (fig. 4.11), a layer of HMDS molecules may be present at the surface of the thermoplastic, as the HMDS-PMMA hydrophobic potential is very similar, possibly due to the presence of a methoxy (-OCH_3) group in the chemical structure of PMMA.

4.2.2 FDTS Results

Measurements of CA for DI water droplets (fig. 4.14a) and PBS droplets (fig. 4.14b) in **PET** surfaces previously exposed to FDTS didn't show a significant variance ($CA_{PET} \simeq 72°$).

Fernández-Blázquez *et al* [70] used different plasma etching ratios to create isolated nanofibrils and fibril bundles on PET substrates and later functionalized the same surfaces with FDTS. For control, a non-plasma treated PET surface was exposed to FDTS by CVD for 2 hours, after which an increment in CA was seen (from 65° to 113°). Although the same technique of silane deposition was used, the exposure time was much higher ($\sim$ 2 h) than the ones explored in this work (between 2 min and 50 min), and a bake step was performed after chemical exposure (75°C for 1 day, under vacuum) to improve the stability of the SAM, which may be key factors for the successful silanization of PET substrates with FDTS.

On the other hand, results regarding **PS** and **PMMA** (fig. 4.14) surfaces showed an increase in contact angle for both substrates. Polystyrene achieved a hydrophobic character (CA_{PS} increased from 88° to $\simeq 100°$) after 20 to 50 min of chemical exposure, while PMMA showed an increase in hydrophobic proneness (CA_{PMMA} increased from 70° to $\simeq$ 87°) reaching a plateau after 10 min of chemical

exposure.

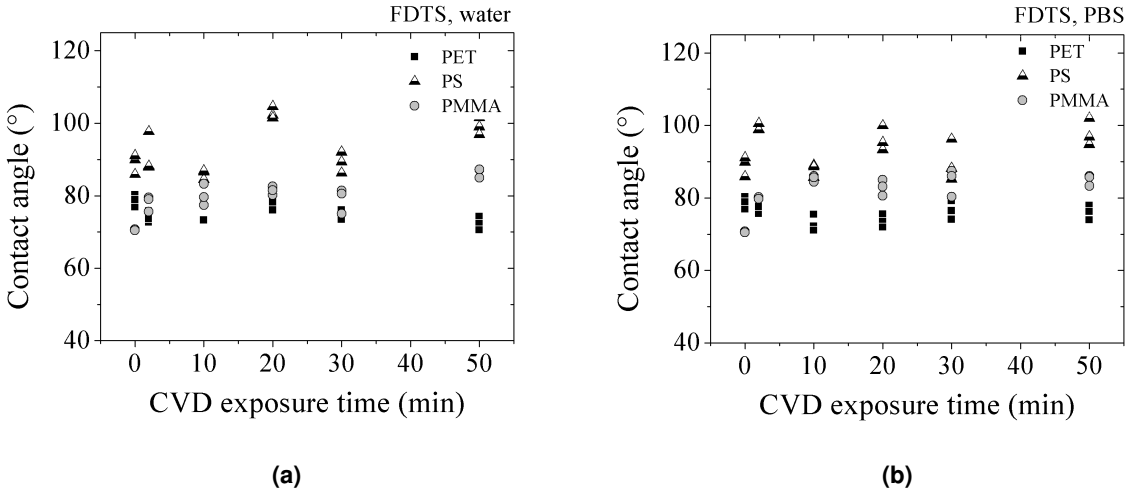

Figure 4.14: Contact angle of **(a)** DI water droplets and **(b)** PBS droplets on rigid surfaces of PET, PS and PMMA thermoplastics after chemical exposure to FDTS by room temperature CVD.

Studies concerning SWM of PS and PMMA surfaces include a prior treatment of the surfaces with oxygen plasma to allow the reaction silane-surface to occur, and no reaction of non-plasma treated surfaces of these thermoplastics and FDTS is described in the literature [71–73]. Despite the increase in CA values, it is assumed that no reaction occurs between PS/PMMA substrates and FDTS molecules, since the chemical groups on each element are not reactive with one another. It is proposed that FDTS molecules rest upon deposition on the substrates by RT-CVD, predominantly in a horizontal orientation (fig. 4.15), exposing difluoromethylene groups (CF_2) which increase the surface energy of PS and PMMA [55].

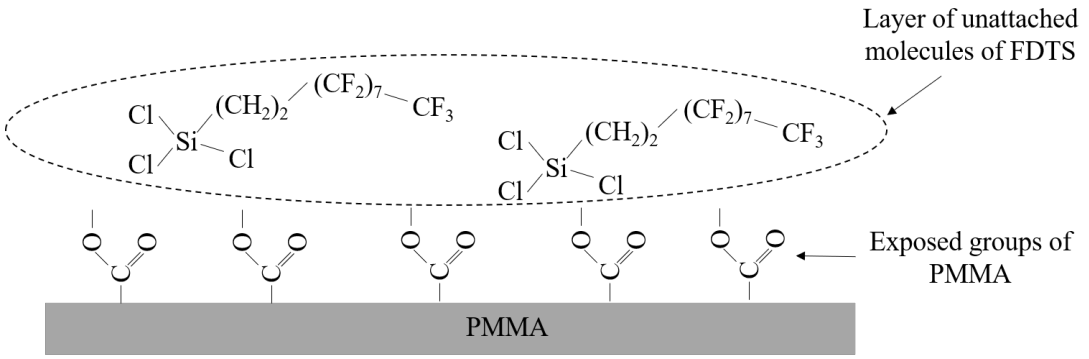

Figure 4.15: Scheme of FDTS molecules on top of PMMA substrates after RT-CVD. Since no FDTS-PMMA reaction occurs, the result is a layer of un-attached molecules of silane.

4.2.3 APTES Results

Results presented in fig.4.16 show that exposure of **PET** and **PS** substrates to APTES vapor lead to a slight increase of CA values, with the increment of exposure time. For 30 min of exposure, CA_{PET}, initially at $\simeq 74°$, increased to $\simeq 100°$, while CA_{PS}, initially at $\simeq 84°$, increased to $\simeq 100°$, the latter after only 10 min activation. As for **PMMA** surfaces, a slight increase in CA was observed with the exposure to APTES silane (CA_{PMMA} initially at $\simeq 67°$, increased to $\simeq 80°$.

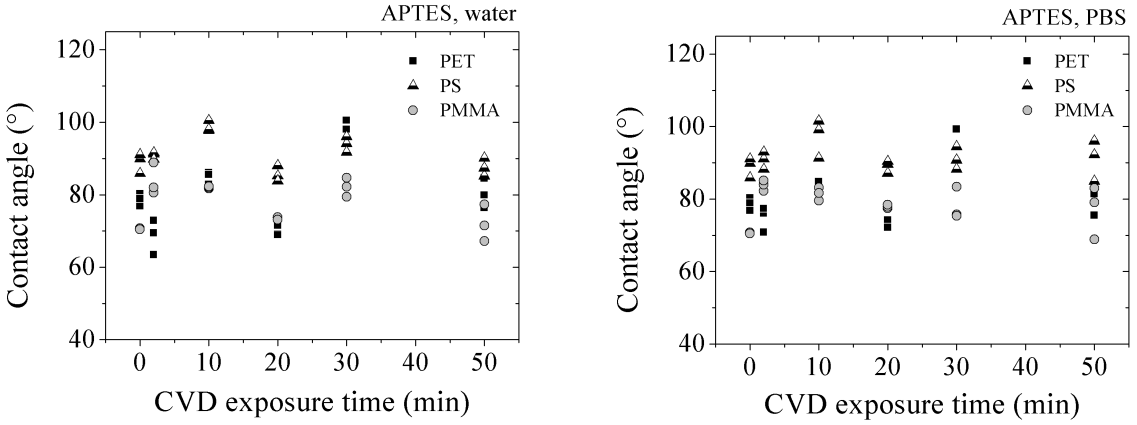

Figure 4.16: Contact angle of **(a)** DI water droplets and **(b)** PBS droplets on rigid surfaces of PET, PS and PMMA thermoplastics after chemical exposure to APTES by room temperature CVD.

Howarter and Youngblood [74] demonstrated the reaction between PET substrates and a liquid-phase of APTES, which relies in two steps. The first step is the establishment of hydrogen bonds among the amine groups of APTES and a H-bond acceptor on the surface of PET (in this case, the double bonded oxygen, fig. 4.10). The second step occurs in the presence of trace volumes of water, where siloxane (Si-O-Si) bonds are formed between near-by APTES molecules, leading to horizontal cross-linking. In this scenario, some molecules of APTES connected by siloxane bonds may not be adsorbed onto the PET surface. However, the horizontal polymerization provides stability to the APTES formed SAM. It is possible that hydrogen-bonds between the amine moieties of APTES and the oxygen atoms of PET substrates were established after 30 min of chemical exposure. However, XPS analysis (not shown) of PET substrates exposed to APTES vapor for 30 min by RT-CVD indicated an absence of APTES molecules on PET surfaces. It is suggested that, due to the ultra high vacuum conditions created upon XPS analysis, the APTES molecules flew off the surface, consequence of the weak character of hydrogen bonds.

A similar reaction might occur for PMMA surfaces, as a hydrogen-acceptor atom (a double-bonded oxygen) is present in its chemical structure (fig. 4.13). The report of Ahn and Lee [75] describes a

new method to bond thermoplastics to PDMS, where the exposure of PET and PMMA surfaces to UV irradiation is followed by functionalization with APTES. In this study, contact angles of both surfaces (before and after the described process) were measured. In the end, the authors obtained PET and PMMA surfaces with the amine groups from APTES exposed away from the surface. However, CA evaluation showed that the values measured did not vary much from the initial non-treated surfaces ($CA_{PET} \simeq 64°$ and $CA_{PMMA} \simeq 73°$). As such, the increase of contact angle observed in fig. 4.16 may result from the exposure of ethoxy groups from APTES molecules consequent of establishment of hydrogen-bonds between the amine moieties of APTES and the oxygen atoms of PMMA , as the hydrophobic potential of ethoxy groups is higher than the hydrophobic potential of amine groups [76]. Variation in measurements of CA for PMMA might result from the presence of a methoxy (-OCH_3) group in its chemical structure, which may influence the orientation of the APTES molecule upon interaction with the surface. In this scenario, fluid molecules would have contact with a lower number of ethoxy groups. Another factor that influences the CA values is the density of silane molecules present in the surface after RT-CVD. It is possible that the measurements of CA obtained for PMMA surfaces are consequent of a APTES coverage of low quality, due to a high dispersion of molecules throughout the surface.

As for PS substrates, in order for a reaction to occur with APTES molecules, the aromatic ring of PS must be activated to stimulate an *ortho/meta* attack by the silane. This method has been applied by Kaur and co-workers [77], who were able to attach carboxylated haptens on PS supports with the usage of APTES as a linker. This method showed great stability and was successfully used in Enzyme-Linked Immusorbent Assays (ELISA). PS plates were treated with a HNO_3 solution in concentrated H_2SO_4 for 30 minutes at room temperature with mild shaking. The acid treatment lead to the formation of nitro-PS in the *para* position of the aromatic ring, which allowed the attack of APTES molecules in an *ortho* position. Since the PS substrates suffered no treatment before exposure to APTES vapor, it is suggested that the increase of CA observed in this work is only a consequence of the deposition of silane molecules, without the occurrence of a chemical reaction.

This preliminary study of SWM of thermoplastics allowed to conclude that functionalization of these substrates was possible with FDTS and APTES (especially PS and PMMA thermoplastics), as an increase of CA values was observed following RT-CVD, due to establishment of hydrogen bonds or simply the presence of unreacted molecules of silane on the substrate. XPS analysis of the chemically exposed surfaces would be pertinent to verify the physical adsorption of silane molecules to the substrates. However, a prior step of UV/O_2 plasma would guarantee the establishment of more stable silane-thermoplastic, specifically covalent bonds, turning the SAM formed on the substrates resistant to cleaning processes.

4.3 Surface material: thin films

Thin films of gold, alumina and silicon dioxide are commonly used in biosensing devices, due to their many advantageous properties, being also implemented in the nanoparticle form. However, some methods of detection with these films may require a previous wettability treatment, to enhance biocompatibility or bioanalite-surface adhesion. Studies of SWM of thin films of gold, alumina and silicon dioxide were performed in the conditions described in chapter 3 and results obtained are discussed below.

4.3.1 HMDS Results

Measurements of CA for DI water drops (fig. 4.17a) and PBS drops (fig. 4.17b) on surfaces of thin films show that SWM with HMDS vapor was more efficient for highly hydrophilic surfaces (alumina thin films) as CA increased from $\simeq 16^\circ$ to $\simeq 100^\circ$, reaching a plateau after 30 min.

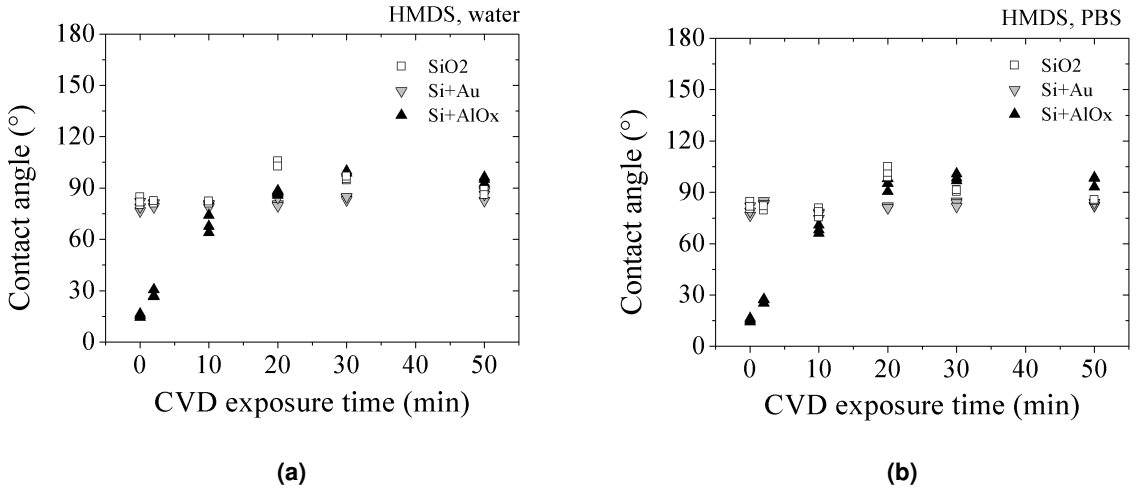

(a) **(b)**

Figure 4.17: Contact angle of **(a)** DI water droplets and **(b)** PBS droplets on thin films of gold, alumina and silicon dioxide after CVD using HMDS.

A decrease of surface energy for **alumina** films was expected, as the surface characteristically displays a layer of hydroxyl groups. Tasaltin *et al* [78] described a new method to prepare superhydrophobic surfaces of alumina by fabrication of a nanoporous structure and exposure to HMDS silane by CVD. For comparation of SWM, the authors exposed a thin film of non-porous alumina to HMDS silane for 4h, at 100°C. After chemical exposure to a vapor-phase of HMDS, a decrease in surface wettability was observed, as the CA increased up to 80°. These results are consistent with the ones obtained in this work with RT-CVD (fig. 4.17) and validate the conclusion of a successful functionalization of alumina thin films with HMDS silane, by exposure of apolar methyl groups. Unlike alumina thin films, **silicon dioxide** thin films showed an initial hydrophobic tendency ($CA_{SiO2,t0}$ = 80°), which indicates that less hydroxyl

groups were available for covalent attachment of HMDS molecules, possibly due to carbonaceous contamination (fig. 4.18) consequent of film aging [79, 80]. A significant increase in CA of SiO_2 films is only observed after 20 min of activation (CA $\simeq$ 100°), which is assumed to be a result of a covalent reaction between the few available hydroxyl groups at the surface and the HMDS molecules.

Figure 4.18: Carbonaceous layer formed on top of SiO_2 thin films due to film aging.

Research regarding silanization of **gold** thin films or gold nanoparticles with alkanethiolates is highly explored in the literature [81, 82]. However, the same can not be said about chemical functionalization with HMDS or FDTS silanes. Functionalization of gold thin films with HMDS or FDTS silanes may be pertinent to improve microfabrication techniques, due to modification of adhesion forces, or to control the behaviour of certain cell types by exposure to different chemical groups (methylated and fluorinated).

Regarding gold surface wettability, an atomic-level clean surface of gold should have a practically null contact angle (CA $\simeq$ 0°) [83]. However, gold surfaces quickly gather carbonaceous contamination [84] when exposed to air or even cleaner environments , such as mercury vacuum (10^{-4} mm) or clean argon atmosphere (1 atm), increasing the surface contact angle (70° $<$ CA $<$ 80°) (fig. 4.19).

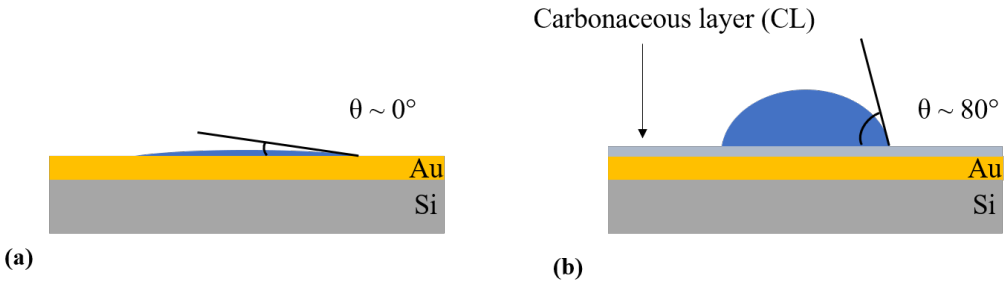

Figure 4.19: Scheme of a droplet of water resting on an **(a)** gold thin film clean at the atomic level and on a **(b)** gold thin film substrate with carbonaceous contamination.

In this work, gold thin films exhibited an initial hydrophobic tendency ($CA_{t0} \simeq 80°$). Additionally, gold thin films have no hydroxyl groups exposed as a result of its non-oxidative character, hence will not react with HMDS. The values of CA obtained might be explained by the similarity in surface energy between the carbonaceous contamination of gold thin films surfaces and the predominant presence of hydrocarbon groups on HMDS molecules deposited on the surface. Of course, this comparation is

dependent on the number of HMDS molecules present in gold thin films surfaces after HMDS deposition by RT-CVD.

4.3.2 FDTS Results

In fig. 4.20, the high hydrophobic potential of FDTS is clearly visible after exposure of **alumina** thin films by RT-CVD, where CA values of DI water and PBS droplets increased from $\simeq 16°$ to $\simeq 95°$ after 10 min of chemical activation which endured over time. The exposure of **silicon dioxide** and **gold** thin films to FDTS lead to an increase in CA measurements of 31% after 10 min and of 25% after 2 min, respectively.

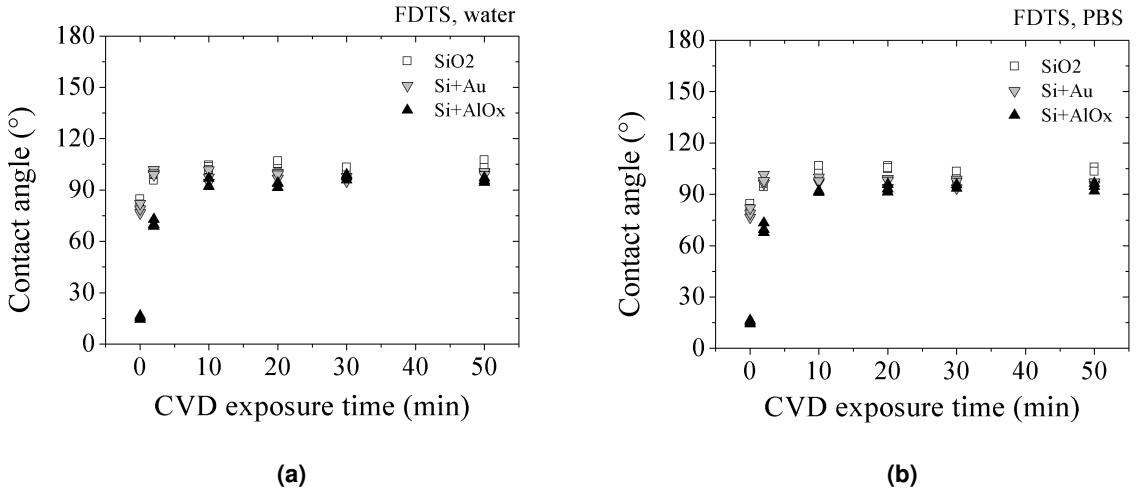

(a) **(b)**

Figure 4.20: Contact angle of **(a)** DI water droplets and **(b)** PBS droplets on thin films of gold, alumina and silicon dioxide after CVD using FDTS.

The establishment of a covalent bond between FDTS molecules and available hydroxyl groups on the surface of **alumina** and **silicon dioxide** thin films occurs, resulting in the exposure of FDTS fluorine groups (CF_n) (fig. 4.21). Although some carbonaceous contamination might be present in SiO_2 films, the hydrophobic potential of FDTS is higher than the potential of the carbon elements, which justifies the increase observed in CA measurements.

As for **gold thin films**, no reaction between FDTS molecules and this material is described in the literature. It is proposed that FDTS molecules rest on top of gold thin films, exposing mostly difluoromethylene groups which also have a higher hydrophobic character than any carbonaceous contamination present in the films. Since activation of gold thin films with FDTS silane lead to practically the same CA threshold value as for SiO_2 and Al_2O_3 thin films, it is assumed that some FDTS molecules, after reaction with the -OH groups present in silicon dioxide and alumina surfaces might be in an horizontal orientation, exposing mainly their $-CF_2$ groups [55]. This assumption is supported by the fact that

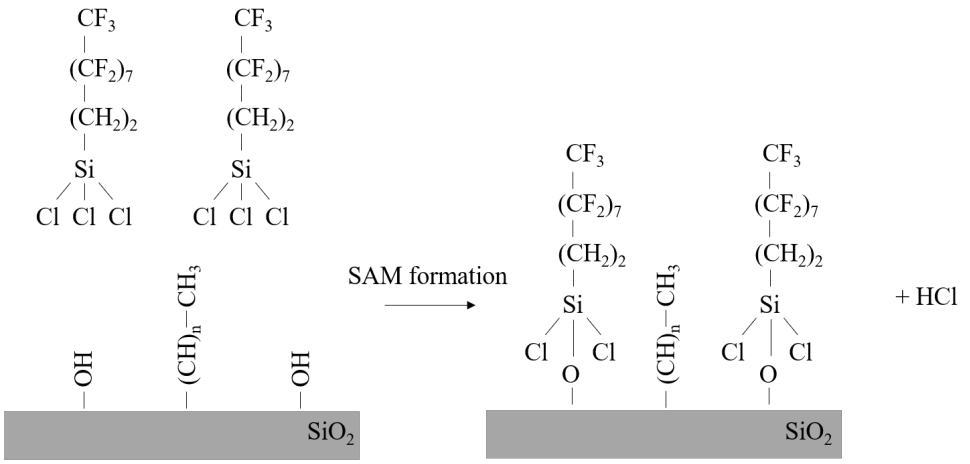

Figure 4.21: Covalent reaction between FDTS molecules and hydroxyl groups present in SiO_2 thin films. The few free hydroxyl groups of silicon dioxide react covalently with the gas-phase FDTS molecules.

it is improbable that all head groups of FDTS react with the disperse -OH groups exposed at the surface without a prior hydrolysis of the FDTS molecules.

4.3.3 APTES Results

Results obtained for DI water droplets (fig.4.22a) and PBS droplets (fig.4.22b) consequent of surface exposure to APTES show that higher CA values were obtained for **silicon dioxide** surfaces (CA increased from $\simeq 80°$ to $\simeq 105°$), changing from an initial hydrophobic tendency to a truly hydrophobic character, which was maintained with the increase of exposure time.

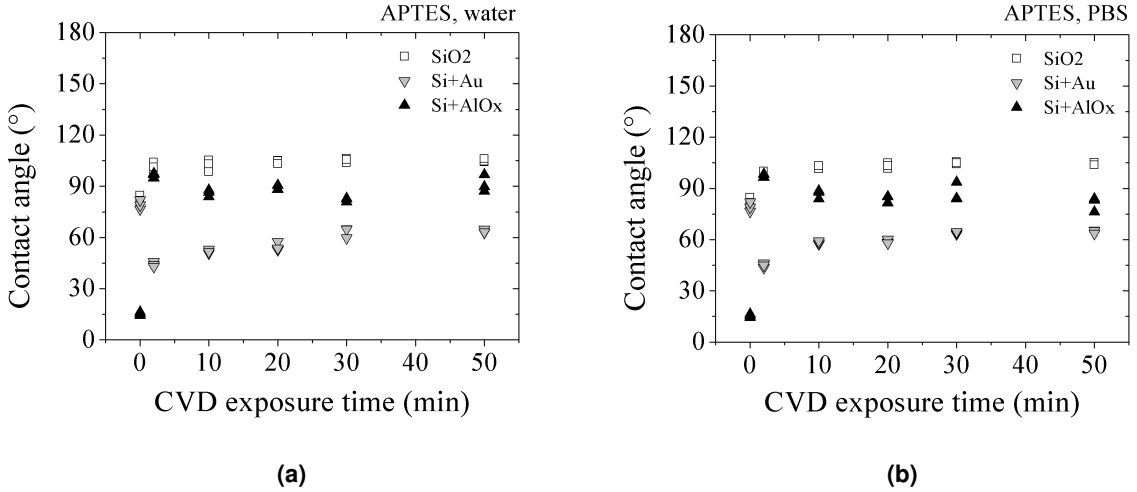

Figure 4.22: Contact angle of **(a)** DI water droplets and **(b)** PBS droplets on thin films of gold, alumina and silicon dioxide after CVD using APTES.

As explained in section 2.2.2.C, ethoxy (EtO) groups present on APTES molecules are expected to react with hydroxyl groups present on the surface, leading to the exposure of amine groups. However, APTES is a very complex silane and the molecules may adopt different orientations depending on the number of ethoxy groups that covalently bond with the surface. Plus, amine groups can establish hydrogen-bonds with existing hydroxyl groups, leading to the exposure of ethoxy groups (2.8).

Yadav, R. A. et al [85] were able to functionalize silicon dioxide surfaces with APTES silane by a vapor-phase deposition method. The substrate exposed to APTES reached a CA value of 40° ± 1°, consequence of the exposure of amine groups. The work of Kyaw, H. H. and co-workers [76] is consisted with these results, in this case in hydrophilic glass surfaces. The authors also indicate that the exposure of three ethoxy groups confers a lower wettability to the surface (comparing to amine groups), followed by the exposure of one (2.8c1)) to two ethoxy groups (2.8c2)), condition of a horizontal molecular orientation. This lead to the conclusion that the increase of CA observed for silicon dioxide surfaces may be a consequence of the exposure of ethoxy groups, which may result from incomplete hydrolysis or establishment of hydrogen bonds (fig. 4.23) between the amine group of APTES and the hydroxyl groups from SiO_2.

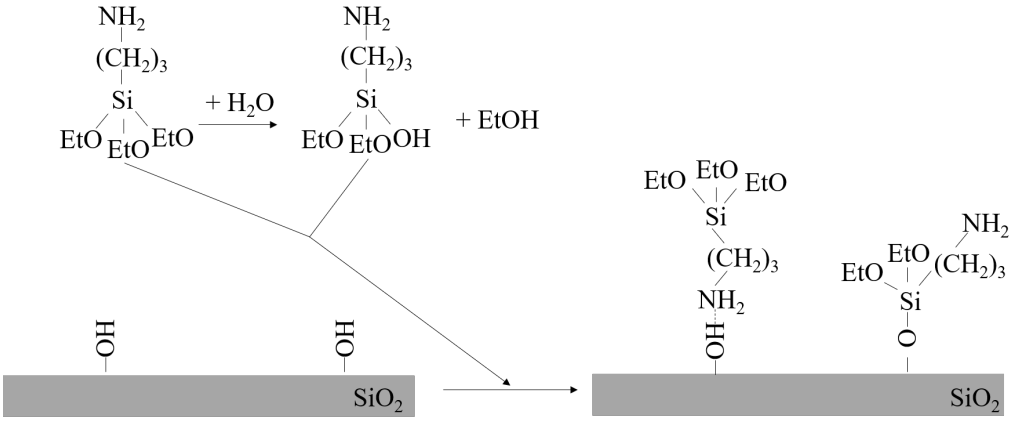

Figure 4.23: Reaction of APTES molecules with silicon dioxide surfaces. Hygroscopic APTES suffers incomplete hydrolysis due to small traces of water, forming hydroxyl groups. The chemical groups establish siloxane bonds, with exposure of the amine group (-NH_2) and the ethoxy groups (-OCH_2CH_3) that did not react with water molecules, leading to a decrease of surface wettability.

As for **alumina** thin films, an increase in contact angle values was observed after exposure to APTES silane (CA reached $\simeq$ 90°). Due to the presence of -OH groups on the surface of these films and the increase of CA observed after chemical exposure, it is proposed that amine moieties of APTES molecules established hydrogen bonds with the free hydroxyl groups at the surface of alumina thin films, exposing the free ethoxy groups of APTES silane. XPS analysis of alumina thin films corroborated this hypothesis and is discussed in section 4.3.3.A.

Chemical exposure of gold thin films ($CA_{gold,t0} \simeq 80°$) to a gas-phase of APTES resulted in a de-

crease of contact angle ($CA_{gold,t2} \simeq 45°$) , which slowly increased with the increment of exposure time, reaching values of $\simeq 64°$ after 50 min. It is well explained in the literature that amine groups establish electrostatic bonds with gold by the free pair of electrons of the nitrogen atom, being the functionalization of hydrophilic surfaces with APTES for the immobilization of gold nanoparticles a common practice [86]. The presence of ethoxy groups on gold thin films following chemical exposure to APTES was expected due to the high amine-gold affinity [87]. For this to be confirmed experimentally, measurements of CA should resemble the values obtained for alumina films, which are consequent of the exposure of ethoxy groups at the surface. However, a decrease in CA measurements was observed, which may indicate that the reaction between APTES molecules and gold thin films was more complex than expected. As mentioned in chapter 2.2.2.C, APTES is a hygroscopic molecule, which means that even trace amounts of water present in the air (humidity) or surfaces leads to molecule hydrolysis and consequent cross-linking between attached APTES molecules. However, the reaction does not necessarily stops there. Even if amine groups adsorb to the gold thin film, hydrolysis of ethoxy groups may lead to a reaction between APTES molecules attached to the film and free APTES molecules present in the vapor-phase, leading to the exposure of amine groups, hydroxyl groups and, in lower number, ethoxy groups. The decrease in CA measurements for gold thin films might be explained by vertical cross-link of APTES, where amine groups are the moieties responsible for the attachment of APTES molecules and decrease of CA values (fig.4.24).

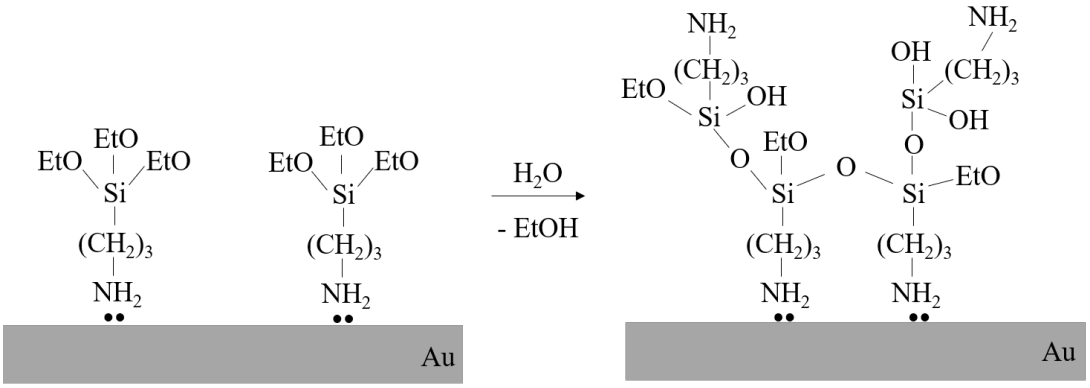

Figure 4.24: Vertical polymerization of APTES molecules in the presence of trace amounts of water, after adsorption to gold thin films. Consequently, a combination of ethoxy (-EtO), hydroxyl (-OH) and amine ($-NH_2$) groups is achieved on the gold surfaces.

Free hydrolysed ethoxy groups (or -OH groups) also contribute to the decrease in CA, due to their polar character. The slight increase of CA with the increment of time can also be explained by this reaction, as the increase of time leads to an increase of ethoxy groups at the surface that did not suffer hydrolysis (as the amount of water in the system is limited to the atmosphere and surface). Of course, results obtained depend on the number of ethoxy groups that suffered hydrolysis and the consequent

orientation adopted by the amine and ethoxy groups.

4.3.3.A XPS Analysis of Alumina Thin Films

Two samples of alumina thin films were analysed by XPS: alumina exposed to APTES by RT-CVD for 30 min and untreated alumina substrates (for control). Samples were analysed at TOA 0º and 60º (angle with the normal to the surface). C 1s, Al 2p, O 1s, N 1s and Si 2p photo-electrons were acquired in detail. The elements which confirm undoubtedly the presence of APTES are the silicon (Si) and nitrogen (N). The spectra obtained for these elements are presented in fig. 4.25.

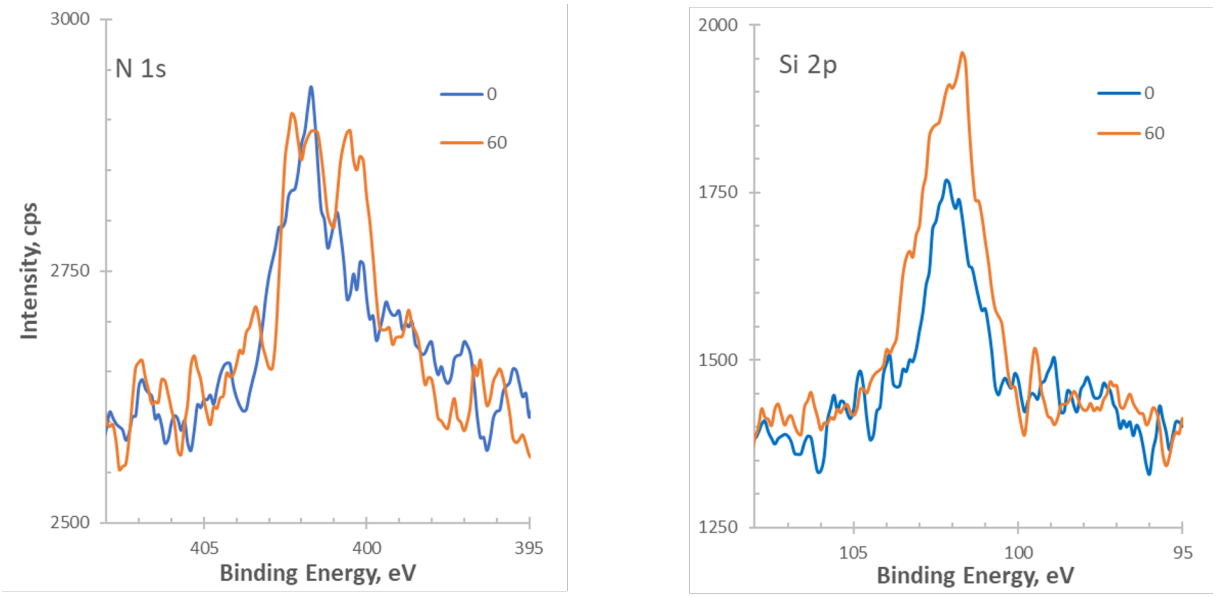

(a) **(b)**

Figure 4.25: (a) N 1s and **(b)** Si 2p XPS regions of Al_2O_3/APTES. Data was smoothed by averaging over 5 points.

Si 2p is a doublet with a spin-orbit split of 0.61 eV, the main component (Si 2p $_{3/2}$) being centred at 101.8 $\pm$ 0.1 eV, typical of Si 2p $_{3/2}$ in siloxanes (Si-O-Si) [88]. N 1s is fittable with two components: 1) 400.4 $\pm$ 0.2 eV and 2) 401.9 $\pm$ 0.2 eV. The first component is assignable to an amine nitrogen [53]. The second one is assigned to a nitrogen with a decreased electronic density; given the BE value, it is possible that a bond N-O was formed [53]. Both N 1s (fig. 4.25a) and Si 2p (fig. 4.25b) intensity increased from 0° to 60°. Since the extreme surface signal is increased at 60°, relatively to the deeper layer, the increase indicates the presence of nitrogen and silicon on the most surficial layer. Furthermore, the quantitative analyses of XPS spectra shows that Si 2p signal increases more than N 1s signal: N 1s/Si 2p (0°) = 0.90 and N 1s/Si 2p (60°) = 0.59. These values are compatible with the nitrogen being, in average, more buried than the silicon in the chemical layer. Within the N 1s region, also a modification of relative intensities of the two components is observed. At 60° the free amine component has a relative

increase suggesting that the N-O component is buried relatively to the free amine. Since the BE values observed for the attached nitrogen situate between BE values of N-O bonds and protonated amines, it is proposed that the nitrogen atoms from APTES established hydrogen bonds with the free hydroxyl groups at the alumina surface. This analysis leads to the reasonable assumption that the increase in CA observed for alumina thin films after chemical exposure to APTES by RT-CVD may be consequent of the exposure of ethoxy groups present in the silane molecules, due to hydrogen-bonding between the amine moieties of APTES and -OH groups from the thin film.

4.4 Surface material: structured silicon dioxide

Deterministic roughness can be obtained by controlling three structure variables that influence the behavior of a liquid droplet on the surface: structure size (*L*), spacing (*d*) and height (*h*). To evaluate the impact of spacing and structure size in surface wettability, square patterns were created by a photolithographic process on silicon dioxide thin films (fig. 4.26a). Square size varied between 1 to 5 μm, while spacing between structures varied between 2 and 5 μm (fig. 4.26b), with a fixed height of 915,8 Å (fig. 4.26c). The nomenclature presented in table 4.2 was used to identify each patterned surface, in which the first number corresponds to the size of the structures (*L*) and the second number is the spacing between the designed square structures (*d*).

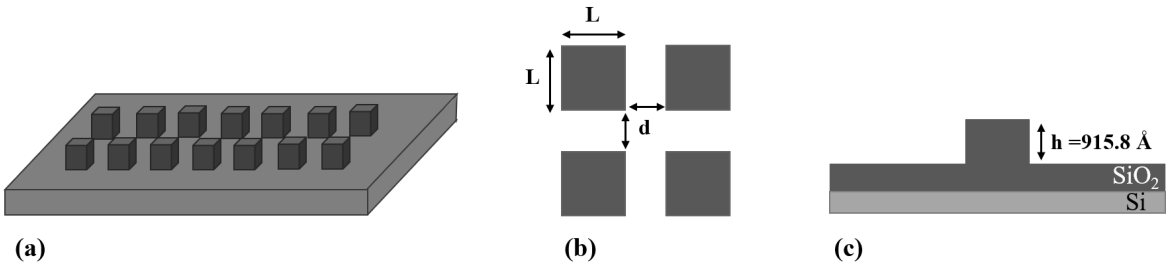

Figure 4.26: Schemes of **(a)** 3D view of the structured pattern designed in SiO_2 thin films (6 x 15 mm, 915.8 Åthick), **(b)** top view of the structures with varying size (1 $\mu m < L <$ 5 μm) and spacing (2 $\mu m < d <$ 5 μm) and **(c)** side view were the height is constant for all structures.

Results presented in fig. 4.27a) and fig. 4.27b) show that all patterned structures decreased the wettability of silicon dioxide thin films, as a truly hydrophobic behavior was observed by increase of CA from 80° (CA of untreated surfaces) to values higher than 90°.

Table 4.2: Nomenclature of the several structures microfabricated in silicon dioxide thin films, where *L* representsthe structure size and d represents the spacing between structures.

Nomenclature	Size, *L* (μm)	Spacing, *d* (μm)
L3d3	3 x 3	3
L5d2		2
L5d3	5 x 5	3
L5d4		4
L1d5	1 x 1	
L2d5	2 x 2	
L3d5	3 x 3	5
L4d5	4 x 4	
L5d5	5 x 5	

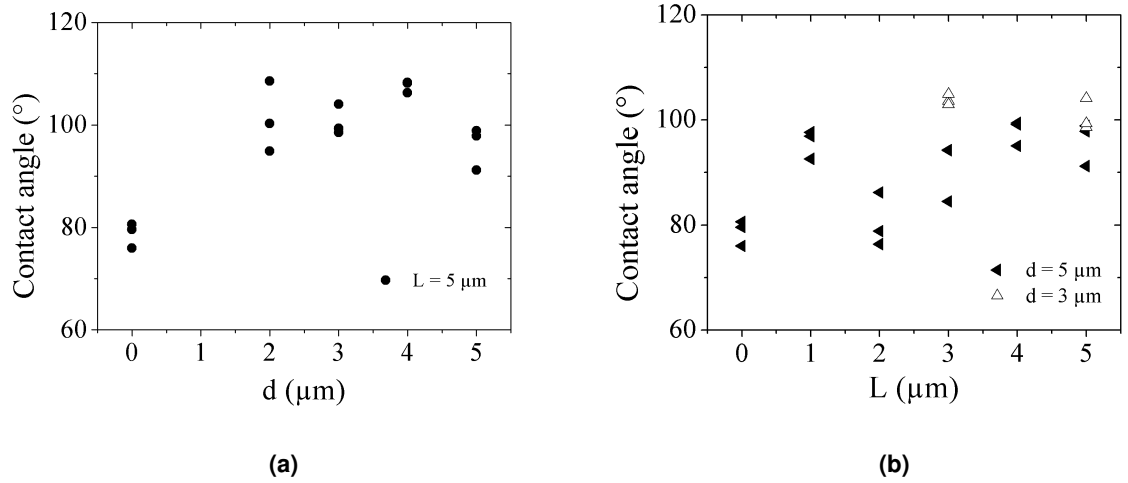

(a) **(b)**

Figure 4.27: CA measurements of DI water droplets on rough surfaces of silicon dioxide with structures of different side size **(a)** and spacing **(b)**.

Variation of spacing (with fixed *L* of 5μm) lead to an increase of CA of 35$\%$, while variation of structure size (with fixed *d* of 5μm) increased CA values by 21,2$\%$. The increase of contact angle or the decrease in surface wettability can be explained by the Cassie-Baxter (CB) model (eq. 2.6), where the increment in surface roughness leads to decrease of surface energy (or decrease in surface wettability), by the presence of air trapped between the structures. The stability of the CB state depends on the vertical force that actuates on a drop on top of a crevice (eq. 4.1), where ΔP is the Laplace pressure (ΔP = P_{liquid} - P_{air}) and A_{aw} is the horizontal projection area [89].

$$F = \Delta P * A_{aw} \tag{4.1}$$

Except for L2d5 structures (fig. 4.27), the weight of 3 μL DI water droplets (chapter 3) was not sufficient to create a high enough hydraulic pressure (P_{liquid}) to surpass the liquid-air energy barrier, thus inhibiting the wetting of the walls of the microfabricated structures [28]. Some authors state that the Cassie-Baxter state is not stable, evolving to a Wenzel state with time, due to thermodynamic instability [89]. This scenario was not explored in this work, nevertheless, the manipulation of physical parameters (such as height, spacing and dimension of structures and critical CB pressure) is a growing field of study as the generation of stable and durable superhydrophobic behavior is a key factor in several applications [90].

By comparing the CA values obtained for fixed *d* (fig. 4.27a) and fixed *L* values (fig. 4.27b), one may notice that the increase in structure size (for a fixed *d* value of 5μm) lead to a decrease in SiO_2 thin film wettability. However, regardless of structure size (*L*), higher CA measurements were achieved for spacing (*d*) values of 2 and 4 μm. For a spacing of 5 μm (L5d5 structure), a decrease of CA was observed (fig. 4.27a). This may indicate that, for the range of values considered in microfabrication, spacing between structures has a higher impact in surface wettability, because the vertical force necessary to surpass the energy-barrier needs to be higher. This results are compatible with the results obtained by Fürstner *et al* [91]. In their work, the impact of square structures of different sizes (1 to 2 μm), spacing (1 to 5 μm) and height (1 to 4 μm) in the wettability of silicon samples was analysed. The authors observed an increase of CA values for silicon surfaces (up to $\simeq 155^{\circ}$) for all structures implemented. It was also observed that, for the same structure size and height, the increase of spacing lead to a decrease in contact angles (e.g. spacing of 5 μm of 1 μm sized structures decreased the CA values to 113°), while an increase in structure size of 1μm lead to a slight decrease in surface wettability.

In this work, the only case where no alteration of CA values was observed was for the L2d5 structures (fig. 4.27b). It is assumed that these structures generate a roughness value similar to the initial roughness of the silicon dioxide thin films, due to the similarity to the $CA_{d0,L0}$ values.

The discrepancy of contact angle values observed for structures L5d2 (fig. 4.28a) and L3d5 (fig. 4.28b) is consequent of some irregularities observed in the pattern by high resolution microscopy.

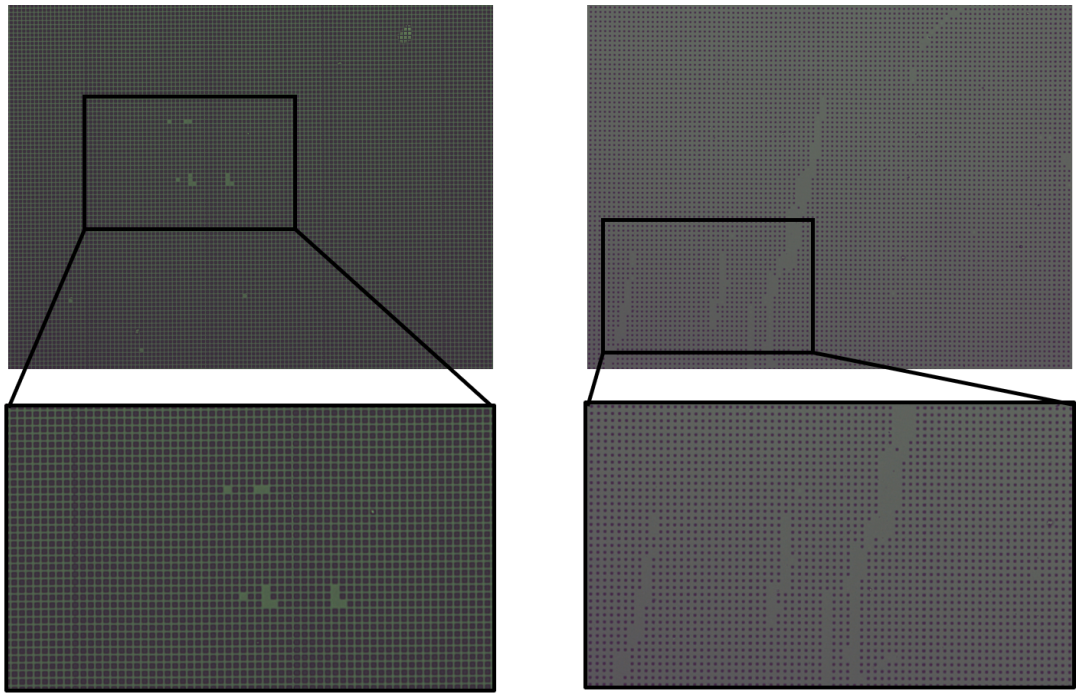

Figure 4.28: Irregularities observed in **(a)** L5d2 and **(b)** L3d5 structures with a 10x amplification.

5

Conclusions

Contents

5.1 Conclusions

The development and optimization of fully integrated microfluidic devices capable of mimic biological processes and to force specific experimental environments has led to the need to control experimental parameters such as surface wettability. SWM, both chemical and physical, is seen as a vital method to control surface wettability. SWM is a process that depends on several parameters: chemical superficial composition of the substrate, surface roughness, chemical modification agent and its hydrophobic/hydrophilic potential, presence of water, temperature, solvent (if a liquid-phase deposition is considered) and pressure (for a vapor-phase deposition). This work made use of two strategies: chemical modification by RT-CVD and physical modification by deterministically altering the surface roughness.

Room temperature CVD was applied to deposit vapor-phases of HMDS, FDTS and APTES in varied classes of materials (silicon, glass, polymers, thin films and thermoplastics).

This technique showed promising results, specially for hydroxyl-containing surfaces. The presence of highly polar groups lead to the covalent attachment of silane molecules and a successful wettability modification. Thus, it is possible to conclude that the presence of adequate surface groups is essential for the formation of a stable SAM on the substrate. Nonetheless, silanization by RT-CVD with HMDS, FDTS and APTES silanes depends on the density of polar groups (in this case, -OH groups) available at the surface for reaction. Results obtained for silanization of thermoplastics indicate the presence of a possible layer of non-reactive silane molecules, which may be useful to prevent the adhesion between substrates without altering the chemical layer of the surfaces. However, results obtained for PET substrates exposed to APTES vapor indicate that the hydrogen-bonds potentially formed between the amine moieties of APTES and the oxygen atom from PET are not very stable, as the XPS analysis indicated an absence of silane molecules on the substrate, possibly due to ultra high vacuum conditions. Therefore, it is preferable to have strongly reactive groups present on the surface to assure the formation of a surface-silane covalent bond, when using RT-CVD, specially if cleaning steps are followed. By comparing the CA values obtained after RT-CVD with the several silanes for oxidized surfaces (Si, glass, SiO_2 and alumina) it is possible to conclude that a threshold for chemical functionalization is obtained earlier (between 2 to 10 min of activation) with FDTS and APTES, which may be justified by their high hydrophobic potential. The only case where this was not observed was for glass surfaces, due to the presence of boron ions on the substrate. Plus, the ability of FDTS and APTES molecules to cross-link with neighbouring unattached silane molecules leads to the formation of more stable SAMs across the substrate. Finally, although a preference for ethoxy groups of APTES to react with hydroxyl groups of the substrate, in liquid-phase silanization, is extensively described in the literature, the same was not observed with exposure to a vapor-phase of APTES. The increase in contact angle measurements of hydrophilic surfaces exposed to this silane indicate a predominance of ethoxy groups, consequent of the establishment of hydrogen-bonds between the amine groups and the polar groups of the substrate. This

scenario was verified by XPS analysis of alumina thin films. Thus, RT-CVD with APTES silane seems favourable to functionalize oxidized surfaces with ethoxy groups.

In conclusion, the results obtained from chemical SWM indicate that the working conditions (-0.78 $\pm$ 0.09 atm of pressure and 22°) are enough for a successful chemical functionalization to occur. This method is also useful to create a non-reactive silane layer on top of the surfaces to avoid the effect of adhesion forces between surfaces in contact.

As for the implementation of deterministic roughness in silicon dioxide thin films, it was verified that the structures designed (except for L2d5 structures) lead to a decrease of surface wettability, which is explained by the Cassie-Baxter model. A higher impact on surface wettability was observed for values of spacing between 2 to 4 μm. However, the design of square patterns withinh the range of 2 to 5 μm showed to be effective in the decrease of surface wettability, leading to a truly hydrophobic behavior. Finally, the use of a photolitographic process enabled the precise control of the dimensions of the pattern, which can be easily reproduced.

5.2 System Limitations and Future Work

Although the results obtained in this work are very promising, the techniques used carry some limitations. The limitation of RT-CVD is the lack of control of trace volumes of water (on the surface and system), which is an important parameter when handling hygroscopic molecules such as APTES. The usage of CA measurements to evaluate SWM was sufficient when chemical reactions occurred after chemical deposition. However, scenarios where a reaction was not foreseen, CA measurements were not sufficient to confirm the presence of silane molecules on the surfaces. A thorough study of surface composition by XPS for a wide spectra of activation times, chemical functionalization agent and surface would be relevant to confirm the presence/absence of silane molecules and the molecule orientation upon contact with the substrate. The effect of a bake step after RT-CVD on chemical stability of the silanes deposited on the surfaces would be interesting to explore, as the increase of temperature may lead to the establishment of more surface-silane covalent bonds or cross-linking between molecules, leading to more stable SAMs. Another pertinent parameter to be evaluated in the future is the activation time, to test if the increase of exposure time will augment the number of covalent bonds consequent of surface-silane reaction.

As for the implementation of deterministic roughness, the design of square patterns with the specified dimensions studied in this work requires photolitography machinery with a very good resolution. The instrument used for microfabrication as a minimum resolution of 0.8 μm, which enables the design of very small structures. The surface L1d5, originally fabricated to contain squares of 1 μm side, showed different shapes from the desired, resembling circles, due to the proximity to the minimum feature size

of the equipment (fig. 5.1). To surpass this limitation, it would be pertinent to test the effects of square patterns of larger dimensions in SiO_2 thin films, to define the limit between the Cassie-Baxter and Wenzel behavior. Wettability studies on other deterministically rough surfaces, such as silicon or different thin films would be interesting, as the creation of superhydrophobic surfaces is a growing field of study in biological and biomedical fields.

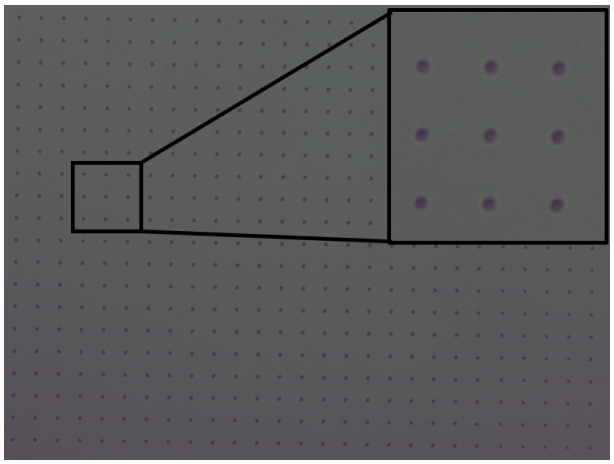

Figure 5.1: Structures of 1x1 μm spaced by 5 μm (50x amplification). The structures obtained resemble circles, instead of the wanted squared structure. This is a consequence of the limit of the photolitography system (0.8 μm).

Bibliography

[1] D. Xu, X. Huang, J. Guo, and X. Ma, "Automatic smartphone-based microfluidic biosensor system at the point of care," *Biosensors and Bioelectronics*, vol. 110, pp. 78–88, 2018. doi: 10.1016/j.bios.2018.03.018.

[2] Y. Zhu, G. Clair, W. B. Chrisler, Y. Shen, R. Zhao, A. K. Shukla, R. J. Moore, R. S. Misra, G. S. Pryhuber, R. D. Smith *et al.*, "Proteomic analysis of single mammalian cells enabled by microfluidic nanodroplet sample preparation and ultrasensitive nanolc-ms," *Angewandte Chemie International Edition*, vol. 57, no. 38, pp. 12 370–12 374, 2018. doi: 10.1002/anie.201802843.

[3] N. Garg, D. Vallejo, D. Boyle, I. Nanayakkara, A. Teng, J. Pablo, X. Liang, D. Camerini, A. Lee, and P. Felgner, "Integrated on-chip microfluidic immunoassay for rapid biomarker detection," *Procedia engineering*, vol. 159, pp. 53–57, 2016. doi: 10.1016/j.proeng.2016.08.063.

[4] M. Tehranirokh, A. Z. Kouzani, P. S. Francis, and J. R. Kanwar, "Microfluidic devices for cell cultivation and proliferation," *Biomicrofluidics*, vol. 7, no. 5, p. 051502, 2013. doi: 10.1063/1.4826935.

[5] R. M. Streicher, M. Schmidt, and S. Fiorito, "Nanosurfaces and nanostructures for artificial orthopedic implants," 2007. doi: 10.2217/17435889.2.6.861.

[6] D. Fan, E. De Rosa, M. B. Murphy, Y. Peng, C. A. Smid, C. Chiappini, X. Liu, P. Simmons, B. K. Weiner, M. Ferrari *et al.*, "Mesoporous silicon-plga composite microspheres for the double controlled release of biomolecules for orthopedic tissue engineering," *Advanced Functional Materials*, vol. 22, no. 2, pp. 282–293, 2012. doi: 10.1002/adfm.201100403.

[7] F. Costantini, R. Tiggelaar, R. Salvio, M. Nardecchia, S. Schlautmann, C. Manetti, H. Gardeniers, G. de Cesare, D. Caputo, and A. Nascetti, "An all-glass microfluidic network with integrated amorphous silicon photosensors for on-chip monitoring of enzymatic biochemical assay," *Biosensors*, vol. 7, no. 4, p. 58, 2017. doi: 10.3390/bios7040058.

[8] X. Wei, V. Q. Do, S. V. Pham, D. Martins, and Y.-A. Song, "A multiwell-based detection platform with integrated pdms concentrators for rapid multiplexed enzymatic assays," *Scientific reports*, vol. 8, no. 1, p. 10772, 2018. doi: 10.1038/s41598-018-29065-7.

[9] B. F. Matarèse, P. L. Feyen, A. Falco, F. Benfenati, P. Lugli *et al.*, "Use of su8 as a stable and biocompatible adhesion layer for gold bioelectrodes," *Scientific reports*, vol. 8, no. 1, p. 5560, 2018. doi: 10.1038/s41598-018-21755-6.

[10] Z. Ma, M. Kotaki, T. Yong, W. He, and S. Ramakrishna, "Surface engineering of electrospun polyethylene terephthalate (pet) nanofibers towards development of a new material for blood vessel engineering," *Biomaterials*, vol. 26, no. 15, pp. 2527–2536, 2005. doi: 10.1016/j.biomaterials.2004.07.026.

[11] N. Chang, J. Zhai, B. Liu, J. Zhou, Z. Zeng, and X. Zhao, "Low cost 3d microfluidic chips for multiplex protein detection based on photonic crystal beads," *Lab on a Chip*, vol. 18, no. 23, pp. 3638–3644, 2018. doi: 10.1039/C8LC00784E.

[12] M. E. Hamdy, M. Del Carlo, H. A. Hussein, T. A. Salah, A. H. El-Deeb, M. M. Emara, G. Pezzoni, and D. Compagnone, "Development of gold nanoparticles biosensor for ultrasensitive diagnosis of foot and mouth disease virus," *Journal of nanobiotechnology*, vol. 16, no. 1, p. 48, 2018. doi: 10.1186/s12951-018-0374-x.

[13] R. Y. Hassan, M. M. Mekawy, P. Ramnani, and A. Mulchandani, "Monitoring of microbial cell viability using nanostructured electrodes modified with graphene/alumina nanocomposite," *Biosensors and Bioelectronics*, vol. 91, pp. 857–862, 2017. doi: 10.1016/j.bios.2017.01.060.

[14] H.-L. Shuai, X. Wu, K.-J. Huang, and Z.-B. Zhai, "Ultrasensitive electrochemical biosensing platform based on spherical silicon dioxide/molybdenum selenide nanohybrids and triggered hybridization chain reaction," *Biosensors and Bioelectronics*, vol. 94, pp. 616–625, 2017. doi: 10.1016/j.bios.2017.03.058.

[15] R. Wolf and A. C. Sparavigna, "Role of plasma surface treatments on wetting and adhesion," *Engineering*, vol. 2, no. 06, p. 397, 2010. doi: 10.4236/eng.2010.26052.

[16] L.-C. Xu and C. A. Siedlecki, "Effects of surface wettability and contact time on protein adhesion to biomaterial surfaces," *Biomaterials*, vol. 28, no. 22, pp. 3273–3283, 2007. doi: 10.1016/j.biomaterials.2007.03.032.

[17] S. M. Oliveira, W. Song, N. M. Alves, and J. F. Mano, "Chemical modification of bioinspired superhydrophobic polystyrene surfaces to control cell attachment/proliferation," *Soft Matter*, vol. 7, no. 19, pp. 8932–8941, 2011. doi: 10.1039/c1sm05943b.

[18] S. Zhan, Y. Pan, Z. F. Gao, X. Lou, and F. Xia, "Biological and chemical sensing applications based on special wettable surfaces," *TrAC Trends in Analytical Chemistry*, 2018. doi: 10.1016/j.trac.2018.09.001.

[19] T. Wassmann, S. Kreis, M. Behr, and R. Buergers, "The influence of surface texture and wettability on initial bacterial adhesion on titanium and zirconium oxide dental implants," *International journal of implant dentistry*, vol. 3, no. 1, p. 32, 2017. doi: 10.1186/s40729-017-0093-3.

[20] V. Silverio, P. A. Canane, and S. C. de Freitas, "Surface wettability and stability of chemically modified silicon, glass and polymeric surfaces via room temperature chemical vapor deposition," *Colloids and Surfaces A: Physicochemical and Engineering Aspects*, 2019. doi: 10.1016/j.colsurfa.2019.03.032.

[21] S. Wang, S. Yu, M. Lu, and L. Zuo, "Microfabrication of plastic-pdms microfluidic devices using polyimide release layer and selective adhesive bonding," *Journal of Micromechanics and Microengineering*, vol. 27, no. 5, p. 055015, 2017. doi: 10.1088/1361-6439/aa66ed.

[22] B. Zhao, C. W. MacMinn, and R. Juanes, "Wettability control on multiphase flow in patterned microfluidics," *Proceedings of the National Academy of Sciences*, vol. 113, no. 37, pp. 10 251–10 256, 2016. doi: 10.1073/pnas.1603387113.

[23] T. Trantidou, Y. Elani, E. Parsons, and O. Ces, "Hydrophilic surface modification of pdms for droplet microfluidics using a simple, quick, and robust method via pva deposition," *Microsystems & Nanoengineering*, vol. 3, p. 16091, 2017. doi: 10.1038/micronano.2016.91.

[24] R. W. A. Oliver, *HPLC of macromolecules: a practical approach*. Oxford University Press on Demand, 1998. doi: 10.1002/jobm.3620300410, vol. 872.

[25] V. Zorba, L. Persano, D. Pisignano, A. Athanassiou, E. Stratakis, R. Cingolani, P. Tzanetakis, and C. Fotakis, "Making silicon hydrophobic: wettability control by two-lengthscale simultaneous patterning with femtosecond laser irradiation," *Nanotechnology*, vol. 17, no. 13, p. 3234, 2006. doi: 10.1088/0957-4484/17/13/026.

[26] J. A. von Fraunhofer, "Adhesion and cohesion," *International journal of dentistry*, vol. 2012, 2012. doi: 10.1155/2012/951324.

[27] Y. Yuan and T. R. Lee, "Contact angle and wetting properties," in *Surface science techniques*. Springer, 2013, pp. 3–34. doi: 10.1007/978–3–642–34 243–1–1.

[28] Q.-S. Zheng, Y. Yu, and Z.-H. Zhao, "Effects of hydraulic pressure on the stability and transition of wetting modes of superhydrophobic surfaces," *Langmuir*, vol. 21, no. 26, pp. 12 207–12 212, 2005. doi: 10.1021/la052054y.

[29] P. Roach, N. J. Shirtcliffe, and M. I. Newton, "Progess in superhydrophobic surface development," *Soft matter*, vol. 4, no. 2, pp. 224–240, 2008. doi: 10.1039/B712575P.

[30] F. Mussano, T. Genova, F. Serra, M. Carossa, L. Munaron, and S. Carossa, “Nano-pore size of alumina affects osteoblastic response,” *International journal of molecular sciences*, vol. 19, no. 2, p. 528, 2018. doi: 10.3390/ijms19020528.

[31] S. Wu, *Polymer interface and adhesion*, 1982. doi: 10.1201/9780203742860.

[32] R. Colorado Jr and T. Lee, “Thiol-based selfassembled monolayers-formation and organization,” *Science and Technology*, vol. 9, p. 9, 2001. doi: 10.1016/B0-08-043152-6/01682-X.

[33] C. Den Besten, R. Van Hal, J. Munoz, and P. Bergveld, “Polymer bonding of micro-machined silicon structures,” in *[1992] Proceedings IEEE Micro Electro Mechanical Systems*. IEEE, 1992. doi: 10.1109/MEMSYS.1992.187699, pp. 104–109.

[34] J. Felbel, I. Bieber, and J. M. Koehler, “Chemical surface management for micro pcr in silicon chip thermocyclers,” in *Biomedical Applications of Micro-and Nanoengineering*, vol. 4937. International Society for Optics and Photonics, 2002. doi: 10.1117/12.468657, pp. 34–41.

[35] V. Jankauskaitė, P. Narmontas, and A. Lazauskas, “Control of polydimethylsiloxane surface hydrophobicity by plasma polymerized hexamethyldisilazane deposition,” *Coatings*, vol. 9, no. 1, p. 36, 2019. doi: 10.3390/coatings9010036.

[36] Z. S. Saifaldeen, K. R. Khedir, M. T. Camci, A. Ucar, S. Suzer, and T. Karabacak, “The effect of polar end of long-chain fluorocarbon oligomers in promoting the superamphiphobic property over multi-scale rough al alloy surfaces,” *Applied Surface Science*, vol. 379, pp. 55–65, 2016. doi: 10.1016/j.apsusc.2016.04.050.

[37] H.-H. Shuai, C.-Y. Yang, I. Hans, C. Harn, R. L. York, T.-C. Liao, W.-S. Chen, J. A. Yeh, and C.-M. Cheng, “Using surfaces to modulate the morphology and structure of attached cells–a case of cancer cells on chitosan membranes,” *Chemical Science*, vol. 4, no. 8, pp. 3058–3067, 2013. doi: 10.1039/C3SC50533B.

[38] P. Saengdee, W. Chaisriratanakul, W. Bunjongpru, W. Sripumkhai, A. Srisuwan, W. Jeamsaksiri, C. Hruanun, A. Poyai, and C. Promptmas, “Surface modification of silicon dioxide, silicon nitride and titanium oxynitride for lactate dehydrogenase immobilization,” *Biosensors and Bioelectronics*, vol. 67, pp. 134–138, 2015. doi: 10.1016/j.bios.2014.07.057.

[39] R. G. Acres, A. V. Ellis, J. Alvino, C. E. Lenahan, D. A. Khodakov, G. F. Metha, and G. G. Andersson, “Molecular structure of 3-aminopropyltriethoxysilane layers formed on silanol-terminated silicon surfaces,” *The Journal of Physical Chemistry C*, vol. 116, no. 10, pp. 6289–6297, 2012. doi: 10.1021/jp212056s.

[40] D. Kwon, H. Yoo, H. Lee, and S. Jeon, “Colorimetric detection of penicillin g in milk using antibody-functionalized dendritic platinum nanoparticles,” *Sensors and Actuators B: Chemical*, vol. 255, pp. 552–556, 2018. doi: 10.1016/j.snb.2017.08.105.

[41] S. Sruthi, A. Loiseau, J. Boudon, F. Sallem, L. Maurizi, P. Mohanan, G. Lizard, and N. Millot, “In vitro interaction and biocompatibility of titanate nanotubes with microglial cells,” *Toxicology and applied pharmacology*, vol. 353, pp. 74–86, 2018. doi: 10.1016/j.taap.2018.06.013.

[42] N. R. Glass, R. Tjeung, P. Chan, L. Y. Yeo, and J. R. Friend, “Organosilane deposition for microfluidic applications,” *Biomicrofluidics*, vol. 5, no. 3, p. 036501, 2011. doi: 10.1063/1.3625605.

[43] J. Creighton and P. Ho, “Introduction to chemical vapor deposition (cvd),” *Chemical vapor deposition*, vol. 2, pp. 1–22, 2001.

[44] C.-Y. Sung, C.-Y. Yang, W.-S. Chen, Y.-K. Wang, J. A. Yeh, and C.-M. Cheng, “Probing neural cell behaviors through micro-/nano-patterned chitosan substrates,” *Biofabrication*, vol. 7, no. 4, p. 045007, 2015. doi: 10.1088/1758-5090/7/4/045007.

[45] A. Alam, M. Howlader, and M. Deen, “The effects of oxygen plasma and humidity on surface roughness, water contact angle and hardness of silicon, silicon dioxide and glass,” *Journal of Micromechanics and Microengineering*, vol. 24, no. 3, p. 035010, 2014. doi: 10.1088/0960-1317/24/3/035010.

[46] H. Craighead, C. James, and A. Turner, “Chemical and topographical patterning for directed cell attachment,” *Current opinion in solid state and materials science*, vol. 5, no. 2-3, pp. 177–184, 2001. doi: 10.1016/S1359-0286(01)00005-5.

[47] D. J. Collins, B. Morahan, J. Garcia-Bustos, C. Doerig, M. Plebanski, and A. Neild, “Two-dimensional single-cell patterning with one cell per well driven by surface acoustic waves,” *Nature communications*, vol. 6, p. 8686, 2015. doi: 10.1038/ncomms9686.

[48] J. Y. Lim and H. J. Donahue, “Cell sensing and response to micro-and nanostructured surfaces produced by chemical and topographic patterning,” *Tissue engineering*, vol. 13, no. 8, pp. 1879–1891, 2007. doi: 10.1089/ten.2006.0154.

[49] A. F. Stalder, T. Melchior, M. Müller, D. Sage, T. Blu, and M. Unser, “Low-bond axisymmetric drop shape analysis for surface tension and contact angle measurements of sessile drops,” *Colloids and Surfaces A: Physicochemical and Engineering Aspects*, vol. 364, no. 1-3, pp. 72–81, 2010. doi: 10.1016/j.colsurfa.2010.04.040.

[50] J. F. Watts, “X-ray photoelectron spectroscopy,” *Surface science techniques*, pp. 5–23, 1994. doi: 10.1016/0042-207X(94)90107-4.

[51] A. C. Ferreira, A. Ferraria, A. B. do Rego, A. P. Gonçalves, M. R. Correia, T. A. Gasche, and J. B. Branco, "Partial oxidation of methane over bimetallic nickel–lanthanide oxides," *Journal of Alloys and Compounds*, vol. 489, no. 1, pp. 316–323, 2010. doi: 10.1016/j.jallcom.2009.09.082.

[52] A. M. Ferraria, A. P. Carapeto, and A. M. B. do Rego, "X-ray photoelectron spectroscopy: silver salts revisited," *Vacuum*, vol. 86, no. 12, pp. 1988–1991, 2012. doi: 10.1016/j.vacuum.2012.05.031.

[53] G. Beamson, "High resolution xps of organic polymers," *The Scienta ESCA 300 Database*, 1992. doi: 10.1021/ed070pA25.5.

[54] B. Arkles, "Hydrophobicity, hydrophilicity and silane surface modification," *Gelest Inc, Morrisville*, 2011.

[55] W. A. Zisman, "Relation of the equilibrium contact angle to liquid and solid constitution," *Contact angle, wettability, and adhesion*, vol. 43, pp. 1–51, 1964. doi: 10.1021/ba-1964-0043.ch001.

[56] B. S. Yilbas, H. Ali, M. R. Yousaf, and A. Al-Sharafi, "2.25 hydrophobic materials," 2018.

[57] M. L. Hair, "Hydroxyl groups on silica surface," *Journal of Non-Crystalline Solids*, vol. 19, pp. 299–309, 1975. doi: 10.1016/0022-3093(75)90095-2.

[58] R. S. Lima, P. A. Leão, M. H. Piazzetta, A. M. Monteiro, L. Y. Shiroma, A. L. Gobbi, and E. Carrilho, "Sacrificial adhesive bonding: a powerful method for fabrication of glass microchips," *Scientific reports*, vol. 5, p. 13276, 2015. doi: 10.1038/srep13276.

[59] G.-Y. Jung, Z. Li, W. Wu, Y. Chen, D. L. Olynick, S.-Y. Wang, W. M. Tong, and R. S. Williams, "Vapor-phase self-assembled monolayer for improved mold release in nanoimprint lithography," *Langmuir*, vol. 21, no. 4, pp. 1158–1161, 2005. doi: 10.1021/la0476938.

[60] Y. X. Zhuang, O. Hansen, T. Knieling, C. Wang, P. Rombach, W. Lang, W. Benecke, M. Kehlenbeck, and J. Koblitz, "Vapor-phase self-assembled monolayers for anti-stiction applications in mems," *Journal of Microelectromechanical Systems*, vol. 16, no. 6, pp. 1451–1460, 2007. doi: 10.1109/JMEMS.2007.904342.

[61] D. Kiaei, A. S. Hoffman, and S. R. Hanson, "Ex vivo and in vitro platelet adhesion on rfgd deposited polymers," *Journal of biomedical materials research*, vol. 26, no. 3, pp. 357–372, 1992. doi: 10.1002/jbm.820260307.

[62] A. Vesel and M. Mozetic, "New developments in surface functionalization of polymers using controlled plasma treatments," *Journal of Physics D: Applied Physics*, vol. 50, no. 29, p. 293001, 2017. doi: 10.1088/1361-6463/aa748a.

[63] D. P. Dowling, F. T. O'Neill, S. J. Langlais, and V. J. Law, "Influence of dc pulsed atmospheric pressure plasma jet processing conditions on polymer activation," *Plasma Processes and Polymers*, vol. 8, no. 8, pp. 718–727, 2011. doi: 10.1002/ppap.201000145.

[64] Y. Arima and H. Iwata, "Effect of wettability and surface functional groups on protein adsorption and cell adhesion using well-defined mixed self-assembled monolayers," *Biomaterials*, vol. 28, no. 20, pp. 3074–3082, 2007. doi: 10.1016/j.biomaterials.2007.03.013.

[65] C. C. Barrias, M. C. L. Martins, G. Almeida-Porada, M. A. Barbosa, and P. L. Granja, "The correlation between the adsorption of adhesive proteins and cell behaviour on hydroxyl-methyl mixed self-assembled monolayers," *Biomaterials*, vol. 30, no. 3, pp. 307–316, 2009. doi: 10.1016/j.biomaterials.2008.09.048.

[66] S. A. Miller and N. E. Leadbeater, "Direct, rapid, solvent-free conversion of unactivated esters to amides using lithium hydroxide as a catalyst," *RSC Advances*, vol. 5, no. 113, pp. 93 248–93 251, 2015. doi: 10.1039/C5RA21394K.

[67] B. Gnanaprakasam and D. Milstein, "Synthesis of amides from esters and amines with liberation of h2 under neutral conditions," *Journal of the American Chemical Society*, vol. 133, no. 6, pp. 1682–1685, 2011. doi: 10.1021/ja109944n.

[68] M. Yildirim, M. Kesimer, N. Hasirci, N. Kilic, and U. Hasanreisoğlu, "Adsorption of human salivary mucin mg1 onto glow-discharge plasma treated acrylic resin surfaces," *Journal of oral rehabilitation*, vol. 33, no. 10, pp. 775–783, 2006. doi: 10.1111/j.1365-2842.2006.01646.x.

[69] Y. Yan, Y. Zhou, L.-B. Huang, S.-T. Han, L. Zhou, Z.-X. Xu, and V. Roy, "Enhanced self-assembled monolayer treatment on polymeric gate dielectrics with ultraviolet/ozone assistance in organic thin film transistors," *RSC Advances*, vol. 5, no. 79, pp. 64 471–64 477, 2015. doi: 10.1039/C5RA13246K.

[70] J. P. Fernández-Blázquez, D. Fell, E. Bonaccurso, and A. Del Campo, "Superhydrophilic and superhydrophobic nanostructured surfaces via plasma treatment," *Journal of colloid and interface science*, vol. 357, no. 1, pp. 234–238, 2011. doi: 10.1016/j.jcis.2011.01.082.

[71] Y. Yuan, S.-O. Choi, and J. Kim, "Analysis of contact area between water and irregular fibrous surface for prediction of wettability," *RSC Advances*, vol. 6, no. 77, pp. 73 313–73 322, 2016. doi: 10.1039/C6RA15389E.

[72] Y. Yuan, M. P. Hays, P. R. Hardwidge, and J. Kim, "Surface characteristics influencing bacterial adhesion to polymeric substrates," *RSC Advances*, vol. 7, no. 23, pp. 14 254–14 261, 2017. doi: 10.1039/C7RA01571B.

[73] L. H. Thamdrup, A. Klukowska, and A. Kristensen, “Stretching dna in polymer nanochannels fabricated by thermal imprint in pmma,” *Nanotechnology*, vol. 19, no. 12, p. 125301, 2008. doi: 10.1088/0957-4484/19/12/125301.

[74] J. A. Howarter and J. P. Youngblood, “Surface modification of polymers with 3-aminopropyltriethoxysilane as a general pretreatment for controlled wettability,” *Macromolecules*, vol. 40, no. 4, pp. 1128–1132, 2007. doi: 10.1021/ma062028m.

[75] S. Ahn and N. Lee, “Solvent-free thermoplastic-poly (dimethylsiloxane) bonding mediated by uv irradiation followed by gas-phase chemical deposition of an adhesion linker,” *Journal of Micromechanics and Microengineering*, vol. 25, no. 7, p. 075007, 2015. doi: 10.1088/0960-1317/25/7/075007.

[76] H. H. Kyaw, S. H. Al-Harthi, A. Sellai, and J. Dutta, “Self-organization of gold nanoparticles on silanated surfaces,” *Beilstein journal of nanotechnology*, vol. 6, no. 1, pp. 2345–2353, 2015. doi: 10.3762/bjnano.6.242.

[77] J. Kaur, K. Singh, M. Raje, G. C. Varshney, and C. R. Suri, “Strategies for direct attachment of hapten to a polystyrene support for applications in enzyme-linked immunosorbent assay (elisa),” *Analytica chimica acta*, vol. 506, no. 2, pp. 133–135, 2004. doi: 10.1016/j.aca.2003.11.009.

[78] N. Tasaltin, D. Sanli, A. Jonáš, A. Kiraz, and C. Erkey, “Preparation and characterization of superhydrophobic surfaces based on hexamethyldisilazane-modified nanoporous alumina,” *Nanoscale research letters*, vol. 6, no. 1, p. 487, 2011. doi: 10.1186/1556-276X-6-487.

[79] M. Chasse and G. Ross, “Effect of aging on wettability of silicon surfaces modified by ar implantation,” *Journal of applied physics*, vol. 92, no. 10, pp. 5872–5877, 2002. doi: 10.1063/1.1516866.

[80] L. Zhang, N. Kuramoto, Y. Azuma, A. Kurokawa, and K. Fujii, “Thickness measurement of oxide and carbonaceous layers on a 28 si sphere by xps,” *IEEE Transactions on Instrumentation and Measurement*, vol. 66, no. 6, pp. 1297–1303, 2016. doi: 10.1109/TIM.2016.2634678.

[81] E. Ostuni, L. Yan, and G. M. Whitesides, “The interaction of proteins and cells with self-assembled monolayers of alkanethiolates on gold and silver,” *Colloids and Surfaces B: Biointerfaces*, vol. 15, no. 1, pp. 3–30, 1999. doi: 10.1016/S0927-7765(99)00004-1.

[82] B. Zhu, T. Eurell, R. Gunawan, and D. Leckband, “Chain-length dependence of the protein and cell resistance of oligo (ethylene glycol)-terminated self-assembled monolayers on gold,” *Journal of Biomedical Materials Research: An Official Journal of The Society for Biomaterials, The Japanese Society for Biomaterials, and The Australian Society for Biomaterials and the Korean Society for Biomaterials*, vol. 56, no. 3, pp. 406–416, 2001. doi: 10.1002/1097-4636(20010905)56:33.0.CO;2-R.

[83] T. Smith, “The hydrophilic nature of a clean gold surface,” *Journal of Colloid and Interface Science*, vol. 75, no. 1, pp. 51–55, 1980. doi: 10.1016/0021-9797(80)90348-3.

[84] M. Chaigneau, G. Picardi, and R. Ossikovski, “Tip enhanced raman spectroscopy evidence for amorphous carbon contamination on gold surfaces,” *Surface Science*, vol. 604, no. 7-8, pp. 701–705, 2010. doi: 10.1016/j.susc.2010.01.018.

[85] A. R. Yadav, R. Sriram, J. A. Carter, and B. L. Miller, “Comparative study of solution–phase and vapor–phase deposition of aminosilanes on silicon dioxide surfaces,” *Materials Science and Engineering: C*, vol. 35, pp. 283–290, 2014. doi: 10.1016/j.msec.2013.11.017.

[86] K. C. Grabar, R. G. Freeman, M. B. Hommer, and M. J. Natan, “Preparation and characterization of au colloid monolayers,” *Analytical chemistry*, vol. 67, no. 4, pp. 735–743, 1995. doi: 10.1021/ac00100a008.

[87] D. Connolly, B. Twamley, and B. Paull, “High-capacity gold nanoparticle functionalised polymer monoliths,” *Chemical Communications*, vol. 46, no. 12, pp. 2109–2111, 2010. doi: 10.1039/b924152c.

[88] A. V. Naumkin, A. Kraut-Vass, S. W. Gaarenstroom, C. J. Powell *et al.*, “Nist x-ray photoelectron spectroscopy database, nist standard reference database 20, version 4.1,” *US Department of Commerce, Washington*, 2012. doi: http://dx.doi.org/10.18434/T4T88K.

[89] H. Gert, N. Foley, D. Zwaan, B. J. Kooi, and G. Palasantzas, “Roughness controlled superhydrophobicity on single nanometer length scale with metal nanoparticles,” *RSC Advances*, vol. 5, no. 36, pp. 28 696–28 702, 2015. doi: 10.1039/c5ra02348c.

[90] H.-Y. Guo, B. Li, and X.-Q. Feng, “Stability of cassie-baxter wetting states on microstructured surfaces,” *Physical Review E*, vol. 94, no. 4, p. 042801, 2016. doi: 10.1103/PhysRevE.94.042801.

[91] R. Fürstner, W. Barthlott, C. Neinhuis, and P. Walzel, “Wetting and self-cleaning properties of artificial superhydrophobic surfaces,” *Langmuir*, vol. 21, no. 3, pp. 956–961, 2005. doi: 10.1021/la0401011.

Anex A